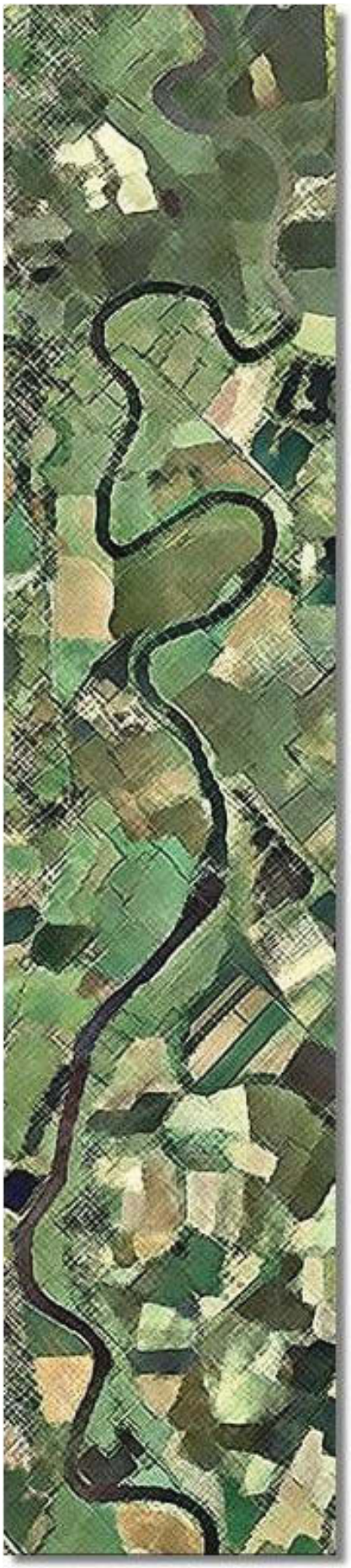

YORK ARCHAEOLOGICAL TRUST

Trent Valley GeoArchaeology 2002

Component 2b: LiDAR Terrain Modelling

Principal Investigator: Keith Challis
York Archaeological Trust

Funded by English Heritage from the Aggregates Levy Sustainability Fund

Environment Agency

Supported by the Environment Agency

www.TVG.org.uk

PNUM 3307

Trent Valley GeoArchaeology 2002

Component 2b: LiDAR Terrain Modelling

Principal Investigator: Keith Challis
York Archaeological Trust

The Trent is a highly mobile river and has left earlier channels scattered across its floodplain. These are a key consideration in the holistic landscape approach to the understanding of the relationship between settlement and the river, to the prediction of certain types of site (such as burnt mounds) to the location of well preserved organic remains and in risk management. Plotting of palaeochannels has been undertaken for the Trent floodplain in Nottinghamshire. Using the techniques established by this work, coverage will be extended to cover the whole Trent Valley area. This will be enhanced by use of LiDAR (Light Detection and Ranging) data for those areas for which it is available. In combination this will provide a levelled surface model of the floodplain.

(Project Outline May 2002)

LIST OF CONTENTS

LIST OF CONTENTS **2**

LIST OF FIGURES **3**

1 INTRODUCTION **6**

2 AIRBORNE LASER ALTIMETRY **7**

2.1 THE LIDAR PRINCIPLE 7
2.2 LIDAR DATA FROM THE ENVIRONMENT AGENCY 7
2.3 COMMISSIONED LIDAR SURVEY 8
2.4 USING EA LIDAR DATA 9
2.5 FILTERING TECHNIQUES 14
2.5.1 High-Pass Filter and Interpolation *14*
2.5.2 Simulated First and Last-Pulse *19*
2.5.3 Effects of Different Interpolation Techniques on Variance Filtered DSM *22*
2.5.4 Conclusions *25*
2.6 REPRESENTING GEOARCHAEOLOGICAL FEATURES 25
2.6.1 User Digitisation *25*
2.6.2 Automatic Feature Extraction *26*
2.6.3 Conclusions *27*

3 THE RIVER TRENT **30**

3.1 INTRODUCTION 30
3.2 THE UPPER TRENT VALLEY 30
3.3 THE MIDDLE TRENT VALLEY 32
3.3.1 Derbyshire *32*
3.3.2 Nottinghamshire *36*
3.4 THE LOWER TRENT VALLEY 40
3.5 LIDAR IN THE TRENT VALLEY: SOME CONCLUSIONS 43

4 THE VALE OF YORK **44**

4.1 INTRODUCTION 44
4.2 THE GEOLOGY OF THE VALE OF YORK *(BY ANDY J HOWARD)* 44
4.3 THE RIVER OUSE 46
4.4 THE RIVER FOSS 46
4.5 LIDAR IN THE VALE OF YORK: SOME CONCLUSIONS 47

5 THE WITHAM VALLEY **50**

5.1 INTRODUCTION 50
5.2 THE GEOLOGY OF THE WITHAM VALLEY 50
5.3 PALAEODRAINAGE OF THE WITHAM VALLEY 50
5.4 ARCHAEOLOGY IN THE WITHAM VALLEY 50
5.5 LIDAR IN THE WITHAM VALLEY: SOME CONCLUSIONS 51

6 CONCLUSIONS **56**

7 REFERENCES **58**

LIST OF FIGURES

Figure 1. Map showing the Trent Valley (1 Upper Trent; 2 & 3 Middle Trent; 4 Lower Trent), (5) Witham Valley and (6) the Ouse and Wharfe river systems in the Vale of York.....10
Figure 2. A single 1km LiDAR tile from the Environment Agency showing (A) solar-shaded digital surface model (DSM), (B) the filter mask used to remove landscape clutter and (C) solar-shaded digital terrain model showing interpolated elevation values filling masked areas. 11
Figure 3. Part of the Lockington Marshes at the confluence of the Rivers Trent and Soar in Leicestershire showing (A) colour-shaded first pulse LiDAR DSM, (B) colour-shaded last-pulse LiDAR DSM, (C) LiDAR laser intensity image (darker equals lower reflectivity) and (D) a conventional aerial photograph of the same area. 12
Figure 4. (A) solar-shaded, (B) colour-shaded and (C) combination colour and solar-shaded unfiltered EA LiDAR DSM of York city centre. Even in this difficult terrain, with extensive opaque ground clutter, it is possible to identify subtle aspects of floodplain topography in the carefully shaded surface model. 13
Figure 5. Diagram showing the various trial processes of filtering and interpolation applied to LiDAR data. 15
Figure 6. 2x2 km LiDAR tile 0416 showing (A) colour and solar shaded unfiltered EA DSM (B) the EA variance filter mask and (C) colour and solar shaded EA interpolated DTM. The line of the profile in Figures 12 and 14 is shown on A in yellow. 16
Figure 7. Filter window cell weights for a McVay high pass convolution filter. 17
Figure 8. Simulated profile through a LiDAR DSM showing the effect of a high-pass filter. Elevation values representing high-frequency (rapid) change (in red) are extracted from the DSM leaving only those values representing low frequency (gradual) change (in green). The filter is effective as high frequency change usually corresponds to buildings, trees and other opaque and semi-opaque objects on the ground surface.....17
Figure 9. 2x2 km LiDAR tile 0416 showing (A) a high-pass filter mask, (B) the DSM with areas of high-frequency elevation change removed, (C) colour and solar shaded 5m resolution DTM interpolated using kriging ,(D) colour and solar shaded 5m resolution DTM interpolated using a local polynomial function and (E) absolute elevation differences between kriged (left) and local polynomial surfaces (right) and the original EA DSM (red lower than original, blue higher than original, green is no change). 18
Figure 10. Effect of resampling from a 2m (unshaded) to a 6m grid resolution (shaded). Each 6m grid cell inherits its value from 9 original cells. 19
Figure 11. 2x2 km LiDAR tile 0416 showing (A) 6m resolution colour and solar shaded simulated first pulse DTM, (B) 6m resolution colour and solar shaded simulated last pulse DTM and (C) elevation differences between simulated first and last pulse (darker is greater difference). 20
Figure 12. Profiles through LiDAR DSM and DTM. (A) unfiltered DSM, (B) EA filtered and interpolated DTM, (C) high pass filter and kriging, (D) high pass filter and local polynomial interpolation and (E) false last-pulse DTM. 21
Figure 13. 2x2 km LiDAR tile 0416 showing (A) unfiltered DSM colour and solar shaded (B) the EA filter mask, colour and solar shaded 2m DTM generated using (C) kriging, (D) IDW and (E) a local polynomial function. 23
Figure 14. Profiles through LiDAR DSM and DTM. (A) DTM interpolated using IDW, (B) DTM interpolated using kriging, (C)) DTM interpolated using a local polynomial function, (D) EA DTM and (E) unfiltered EA DSM. 24
Figure 15. (A) LiDAR DSM of a part of the Witham Valley in Lincolnshire showing sinuous relict channels as raised roddens and creek ridges. (B) the same data threshold ed. The majority of the relict channels are isolated by this method, and are relatively easily extracted automatically, however, some modern landscape detail remains.....28
Figure 16. (A) LiDAR DSM showing ridge and Swale and flood thalwegs within meander core of the Trent at Gonalston, Nottinghamshire. In this case the relict channels are defined by slight depressions in the surface. (B) thresholded view of the same data, the relict channels are more clearly defined, but still elude automatic extraction. 29
Figure 17. Colour-shaded LiDAR DSM of the Upper Trent Valley at Great Heywood showing details of palaeochannels within the floodplain and the location of core sample 1 taken by Havelock and Howard. 31
Figure 18. Map showing the floodplain (yellow) and terraces (brown) of the Middle Trent Valley between the Rivers Dove and Derwent. 33

Figure 19. Colour-shaded LiDAR DSM of the Middle Trent Valley between the Rivers Dove and Derwent. 33
Figure 20. The Middle Trent Valley centred on Twyford, Derbyshire showing the Geological Survey mapping of the drift geology of the terraces and floodplain with palaeochannels mapped from air-photos superimposed. 34
Figure 21. Colour-shaded LiDAR DSM of the area shown in Figure 20. The principal units of the drift geology are clearly evident, as is a mass of additional detail of the geomorphology of the terraces and floodplain. The Locations of core samples of palaeochannels taken by Havelock and Howard are shown. 34
Figure 22. Map showing the floodplain and terraces of the Middle Trent Valley between the Rivers Dove and Derwent with the locations of palaeochannels plotted from air-photographs shown in grey. 35
Figure 23. Map showing the floodplain and terraces of the Middle Trent Valley between the Rivers Dove and Derwent with the locations of palaeochannels plotted from LiDAR data shown in grey. 35
Figure 24. Map showing the floodplain (yellow) and terraces (brown) of the Middle Trent Valley at Gunthorpe. 37
Figure 25. Colour-shaded LiDAR DSM of the Middle Trent at Gunthorpe. The complex geomorphology of the floodplain and terraces is clearly evident. 37
Figure 26. Map showing the floodplain and terraces of the Middle Trent valley at Gunthorpe with the locations of palaeochannels plotted from air-photographs shown in grey. 38
Figure 27. Map showing the floodplain and terraces of the Middle Trent valley at Gunthorpe with the locations of palaeochannels plotted LiDAR data shown in grey. 38
Figure 28. Colour-shaded DSM of the Middle Trent Valley at Gunthorpe showing sinuous palaeochannel of the Trent and a complex arrangement of ridge and swale and probable flood thalwegs within a meander core. The location of core sample 7 taken by Havelock and Howard is also shown. 39
Figure 29. Colour-shaded DSM of the Middle Trent Valley at between Caythorpe and Gunthorpe showing a substantial flat-bottom trough now followed by Car Dyke, but perhaps an earlier course of the Trent and multiple channels, perhaps vestiges of an early Holocene braid-plain. 39
Figure 30. Map showing the drift geology of the Lower Trent Valley at the confluence of the Rivers Trent and Idle. 41
Figure 31. Colour-shaded LiDAR DSM of the Lower Trent Valley at the confluence of the Rivers Trent and Idle. 41
Figure 32. Colour-shaded LiDAR DSM of the Lower Trent Valley at the confluence of the Rivers Trent and Idle. The raised levee of the contemporary Trent channel and palaeodrainage features in the surrounding peatlands is clearly evident. 42
Figure 33. Colour-shaded LiDAR DSM of the Lower Trent Valley at the confluence of the Rivers Trent and Idle. A substantial rodden marking an earlier course of the River Trent is clearly visible. A number of circular features in the south-east of the image (within yellow square) are reminiscent of round barrows revealed by shrinking peat. 42
Figure 34. Colour-shaded pseudo-3D view of an extract from the LiDAR DSM of the Lower Trent Valley showing circular features reminiscent of round barrows revealed by shrinking peat (see Figure 33 for location of extract). 43
Figure 35. The drift geology of the Vale of York, showing the three LiDAR study areas discussed in the text: (1) the Ouse/Wharfe confluence (2) the Ouse at Naburn and (3) The River Foss. 45
Figure 36. Colour-shaded LiDAR DSM of the confluence of the Rivers Wharfe and Ouse at Cawood. The floodplains of these two rivers are dominated by the accretion of fine-grained alluvial silt and clay and few palaeochannels are evident along their length. The linear ride of the Escrick moraine is clearly visible in the centre of the image. 48
Figure 37. Colour-shaded LiDAR DSM of the Ouse Valley at Naburn., south of York with cropmarks from the English Heritage National Mapping Programme superimposed LiDAR clearly reveals subtle variations in the topography of the floodplain and terraces mirroring underlying geology and affecting cropmark formation. 48
Figure 38. Colour-shaded pseudo-3d view of LiDAR DSM of the Valley of the River Foss and its tributaries the Osbaldwick Beck and Tang Hall Beck to the north-east of York. Details of these Valleys, largely submerged by the suburban growth of York, together with the subtle surface topography of aeolian dune deposits are evident. 49

Figure 39. LiDAR coverage of the Witham Valley between Fiskerton and Conningsby shaded to show palaeodrainage in the valley floor. The detailed areas shown in Figures 40 to 44 are highlighted in red.....52
Figure 40. Greyscale LiDAR DSM of the Witham Valley at (left) Branston and (right) Blankney. A complex palaeodrainage system is revealed by slightly raised roddens and creek ridges emerging from the desiccating and shrinking peat that covers the floodplain.....53
Figure 41. Greyscale LiDAR DSM of the Witham Valley. Bronze Age round barrows of the Barlings barrow cemetery are visible as raised (lighter colourer) areas. 53
Figure 42. Greyscale LiDAR DSM of the Witham Valley at Fiskerton. The complex geomorphology of the floodplain is clearly evident. A number of Bronze Age round barrows emerging from the desiccating and shrinking peat are visible as slightly raised (lighter coloured) areas in the south-east of the image. See Figure 30 for pseudo-3D view of outlined area. 54
Figure 43. Colour-shaded pseudo-3D view of and extract of the LiDAR DSM of the Witham Valley showing the barrow group seen in Figure 42.....55
Figure 44. Woodhall Spar DMV, Lincolnshire. A comparison of solar-shaded LiDAR DSM and vertical air-photography shows the effectiveness of LiDAR for identifying and mapping archaeological earthworks. 55

1 INTRODUCTION

This component of Trent Valley GeoArchaeology 2002 aims to examine the potential use of airborne laser altimetry (commonly LiDAR, an acronym for Light Detection and Ranging) for geoarchaeological prospection, principally in the alluvial landscape of the River Trent. The study uses data provided by the United Kingdom Environment Agency (EA) for the Trent Valley and for two other river corridors in the midlands and north of England: the River Ouse, in the Vale of York, North Yorkshire and the River Witham in Lincolnshire (Figure 1). These areas represent varied environments including upper middle and lower/perimarine river reaches and are therefore likely to give a good account of any variations in the efficacy of LiDAR in different river reaches.

Some additional LiDAR data, collected in a commissioned study of a small part of the Middle Trent at Lockington in Leicestershire, allowed comparison of variations in spatial resolution and other sensor properties with the standard data product provided by EA.

Archaeological uses of LiDAR have been examined in several previous studies (Barnes 2003; Bewley 2003). LiDAR is frequently used as a tool for examining aspects of river floodplains, most often for geomorphological or flood prediction purposes (Lohani and Mason 2001; Charlton *et al* 2003; Cobby *et al* 2001; Marks and Bates 2000), but also for such varied applications as shallow water bathymetry (Guenther *et al* 2000) and automatic mapping of sand dune morphology (Rango *et al* 2000). The present study was specifically aimed at investigating the potential of LiDAR as a tool for geoarchaeological prospection in alluvial landscapes. The study had the following objectives:

- To investigate the mapping of geomorphological features such as palaeochannels.
- To refine mapping of river terrace and floodplain for example in order to identify areas of potential for preservation and erosion.
- To identify variations in floodplain and terrace microtopography likely to indicate favourable locations for past activities.
- To investigate potential to identify cultural archaeological and landscape features.

In order to test its efficacy, LiDAR data was compared with existing geological mapping and results obtained from conventional techniques such as analysis of air-photographs.

Section two of this paper briefly reviews the technical aspects of airborne laser altimetry before critically assessing EA LiDAR and discussing some aspects of image processing LiDAR data. In sections three to five each of the study areas is reviewed in turn. Section six presents some overall conclusions on the efficacy of LiDAR in alluviated landscapes.

2 AIRBORNE LASER ALTIMETRY

2.1 The LiDAR Principle

Airborne laser altimetry uses the properties of coherent laser light coupled with precise kinematic positioning provided by a differential global positioning system (DGPS) and inertial attitude determination provided by an inertial measurement unit (IMU) to produce horizontally and vertically accurate elevation measurements.

The laser, most often a pulse laser measuring at rates in excess of 30 MHz, projects a coherent beam of light at the ground surface, the reflection of which is recorded by a sensitive receiver. The laser light is projected through a swath beneath the moving aircraft, usually through the use of rotating mirrors. The spatial resolution scanning laser and swath width are determined as a product of the frequency of laser pulse and altitude of the aircraft at the time of survey. Travel times for the pulse/reflection are used to calculate distance from laser to reflecting object. Typically the receiver is able to record multiple returns for a single pulse, allowing recording for example of a partial return from the top of a semi-opaque object such as a woodland canopy and from the opaque ground beneath the canopy. Other information, such as the intensity (amplitude) of the reflection may also be recorded.

The DGPS provided detailed three-dimensional information on the location of the laser unit, while the IMU provides information on the pitch, roll and yaw of the aircraft. The complete system comprises a scanning laser unit coupled with a DGPS and IMU linked through a computerised control monitoring and recording unit.

Post-survey processing of the simultaneously recorded laser, location and attitude data allows reconstruction of elevation values for the ground surface. Raw survey data are in the form of a cloud of x,y,z point, these are usually projected to a local map datum, sorted, filtered and used to generate a regular raster array of elevation values.

A detailed technical discussion of scanning laser altimeters may be found in Wehr and Lohr (1999), while details of the system used in the present study is contained in Optech 2003.

2.2 LiDAR Data from the Environment Agency

The majority of the LiDAR data used in the present study were supplied by the Environment Agency. EA LiDAR data have been collected principally as part of the Agency's remit to provide flood prediction and management information. Data are gathered as part of an integrated airborne remote sensing system using an Airborne Laser Terrain Mapper (ALTM) the Optech ALTM 2033 LiDAR (Brown *et al* 2003) typically collecting 0.5 points/m2. The raw LiDAR data are processed to WGS84 projection, transformed to British National Grid and a regular grid array, with elevation values at grid nodes, generated from the raw point-could.

LiDAR record the height of both the ground surface and all opaque and semi opaque ground surface objects. The LiDAR laser pulse is reflected from the land surface and opaque objects, such a buildings resting on the ground surface. However, in the case of semi-opaque objects such as trees and vegetation some laser light is reflected from the top of the tree canopy or vegetated surface while some laser light passes through

the tree canopy or vegetation cover to be reflected from the underlying ground surface. It is possible to isolate these discrete reflected data into first-pulse (FP: from top of tree canopy, opaque ground cover and land surface) and last-pulse (LP: ground surface beneath tree cover, etc.) laser returns. Unfortunately EA's standard data product does not provide access to FP and LP data.

Clutter-laden LiDAR data, containing all land surface details, are usually referred to as a digital surface model (DSM). These data are often manipulated before use to remove landscape clutter and insert elevation values representing a bare-earth land surface, usually referred to as a digital terrain model (DTM). A number of methods may be employed to achieve this end result. EA use a 3x3 variance filter to identify areas of the DSM above a threshold limit (set at a 66.6 degree slope gradient). These areas are buffered and the resulting mask used to remove areas of the DSM which are replaced by interpolating new elevations across the gaps (Marks and Bates 2000, 2112; Priestnall *et al* 2000, 71). The filter itself is highly effective at identifying landscape clutter, however, the interpolation process used to fill the resulting holes in the elevation data is problematic and the DTM usually includes significant interpolation artefacts. EA's standard data product includes unfiltered DSM (Figure 2A), the filter layer (Figure 2B) and filtered DTM with interpolated bare-earth elevation values (Figure 2C).

2.3 Commissioned LiDAR Survey

Data from a commissioned LiDAR survey of a part of the floodplain of the Rivers Trent and Soar at their confluence at Lockington Marshes, Leicestershire was also available for examination. The survey was undertaken by Infoterra (www.infoterra-global.com) using an identical instrument to that used by EA (an Optech 2033 LiDAR). The Infoterra survey provided access to raw point-cloud, data as well as FP and LP and laser intensity (Figure 3). Initial processing of the point-cloud data was undertaken by Steve Wilkes of the Visual and Spatial Technology Centre, at Birmingham University; point cloud data were used to generate DSM by surfacing using a rubber sheeting algorithm to produce a regular grid. Work was undertaken in ERDAS Imagine image processing software.

Comparison of interpolated surfaces produced from first pulse (Figure 3A) and last pulse (Figure 3B) laser returns suggest that, at least in landscapes with moderate semi-opaque ground cover (compare LiDAR with aerial photograph in Figure 3D) LiDAR is effective in penetrating tree cover to reveal underlying land surface, and that access to last-pulse returns provides a significant improvement over techniques requiring filtering and interpolation to produce a DTM.

The reflected laser intensity data (Figure 3C) provides an indication of the intensity of reflection of the laser pulse. Initial examination of this data suggests that there is a fall-off in the intensity of the reflected light that corresponds with landscape features such as palaeochannels. Variations in the reflectivity of various earth surface materials to laser light of differing wavelength are quite well documented (for example see Wehr and Lohr 1999, 74) and damp soil conditions are known to reduce reflectivity. It is possible that the increased soil-moisture associated with palaeochannels and perhaps other associated variations in soil and vegetation properties, are responsible for the reduced reflectivity of the laser pulse. This

phenomenon is untested, but worthy of further examination as if reflected laser intensity is indeed related to soil moisture it may provide a useful means to identify waterlogged features likely to be of greater palaeoecological significance, or even the slight variations in soil moisture that are responsible for the formation of archaeological cropmarks.

2.4 Using EA LiDAR Data

LiDAR data from EA is supplied 2km square tiles with a 2m grid resolution in ESRI ASCII grid format. Data were prepared for use by importing the individual tiles into ArcGIS and merging them to form larger DSM representing the entire of each river reach studied.

LiDAR DSM are commonly visualised using solar-shading to highlight variations in topography (Figure 3A; *cf* Charlton *et al* 2003, figs.1 and 3). This technique is effective in visualising gross topographic variation over large areas, particularly where underlying height trends prevent more subtle shading. However solar-shading is less able to highlight minor variations of elevation, in the order of decimetres, typical of archaeological features of floodplains such as palaeochannels.

In the present study solar-shading was supplemented by careful colour-shading of each reach-scale DSM to reveal minor variations in topography (Figure 3B). Elevation values were processed using either a contrast stretch or a histogram equalisation algorithm to enhance shading (Mather 1999). In practice it often proved necessary to restrict analysis and shading to a restricted range of elevation values representing only those parts of the floodplain and terraces of each river reach forming the focus of study. This allowed the full colour-ramp to be used for this limited range of elevation values but required that areas of higher elevation were not visualised.

In longer river reaches the gradual fall in base elevation values along the valley meant that colour-shaded visualisation of the entire reach at a single episode was not feasible and the reach was divided into smaller block for shading and visualisation (Lohani and Mason 2001, 106).

Both monochrome and polychrome colour-ramps were used and these were combined with a semi-transparent solar-shaded overlay to enhance visualisation of topographic detail (Figure 3C).

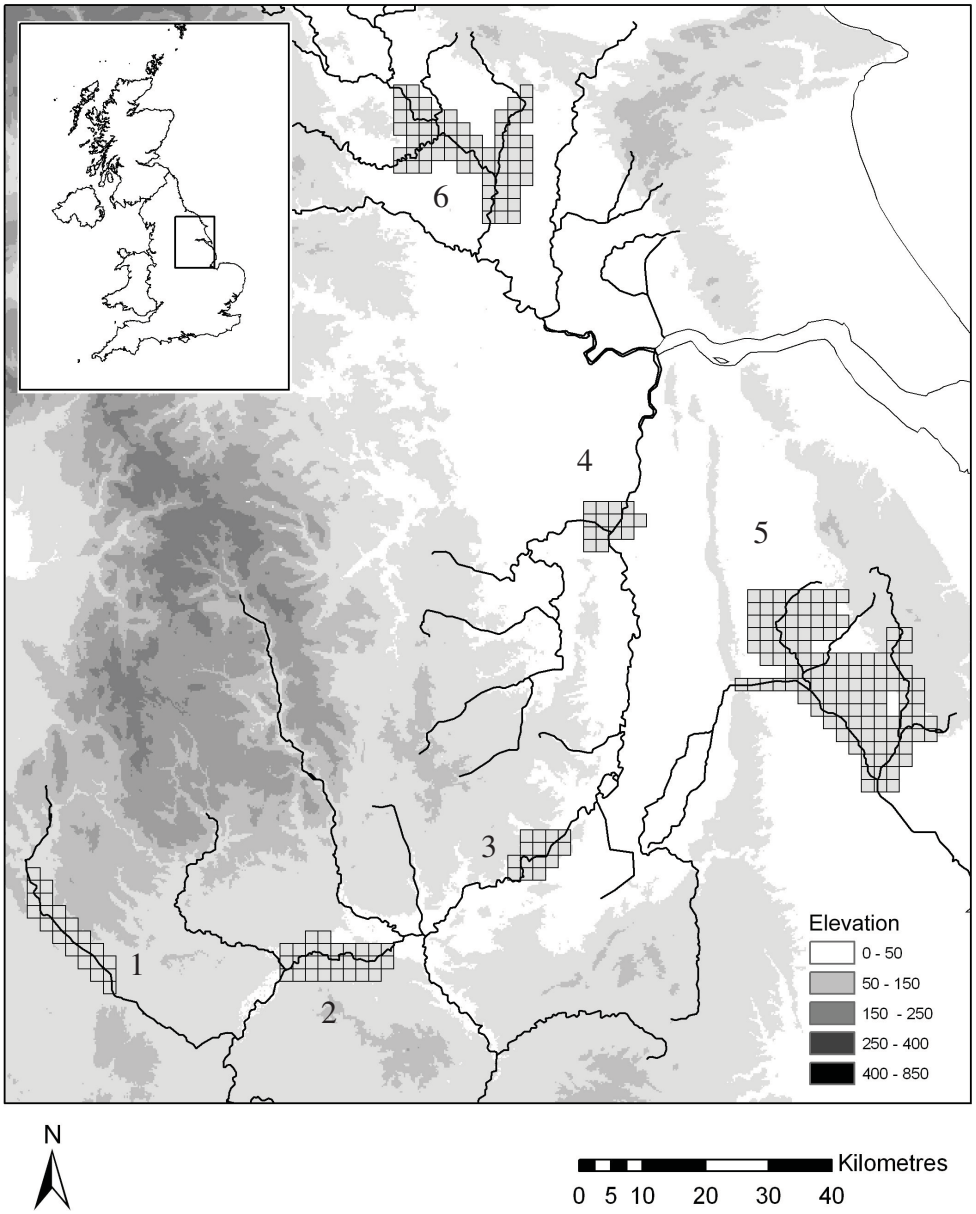

Figure 1. Map showing the Trent Valley (1 Upper Trent; 2 & 3 Middle Trent; 4 Lower Trent), (5) Witham Valley and (6) the Ouse and Wharfe river systems in the Vale of York.

A

B

C

Figure 2. A single 1km LiDAR tile from the Environment Agency showing (A) solar-shaded digital surface model (DSM), (B) the filter mask used to remove landscape clutter and (C) solar-shaded digital terrain model showing interpolated elevation values filling masked areas.

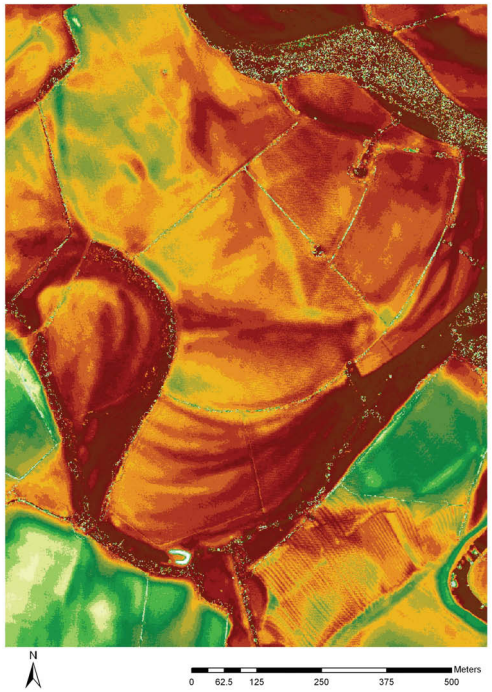

A

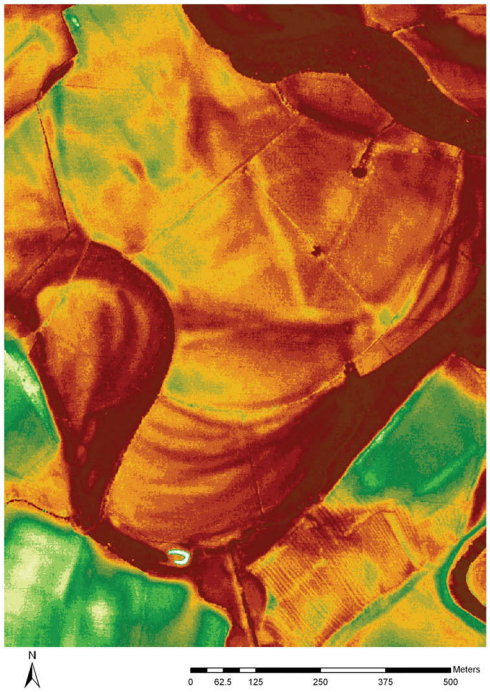

B

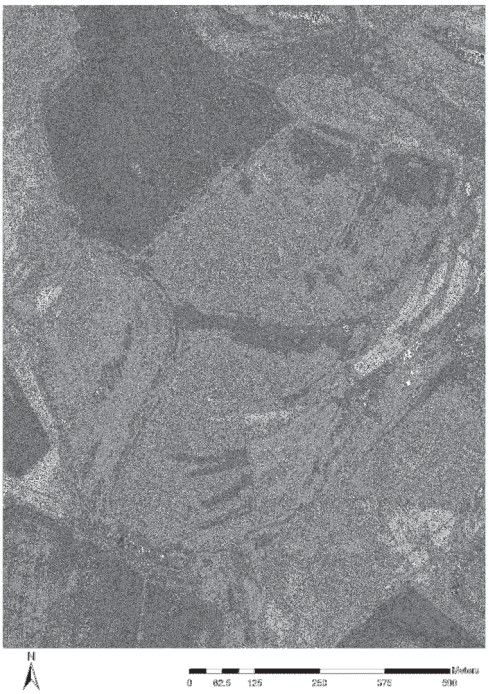

C

D

Figure 3. Part of the Lockington Marshes at the confluence of the Rivers Trent and Soar in Leicestershire showing (A) colour-shaded first pulse LiDAR DSM, (B) colour-shaded last-pulse LiDAR DSM, (C) LiDAR laser intensity image (darker equals lower reflectivity) and (D) a conventional aerial photograph of the same area.

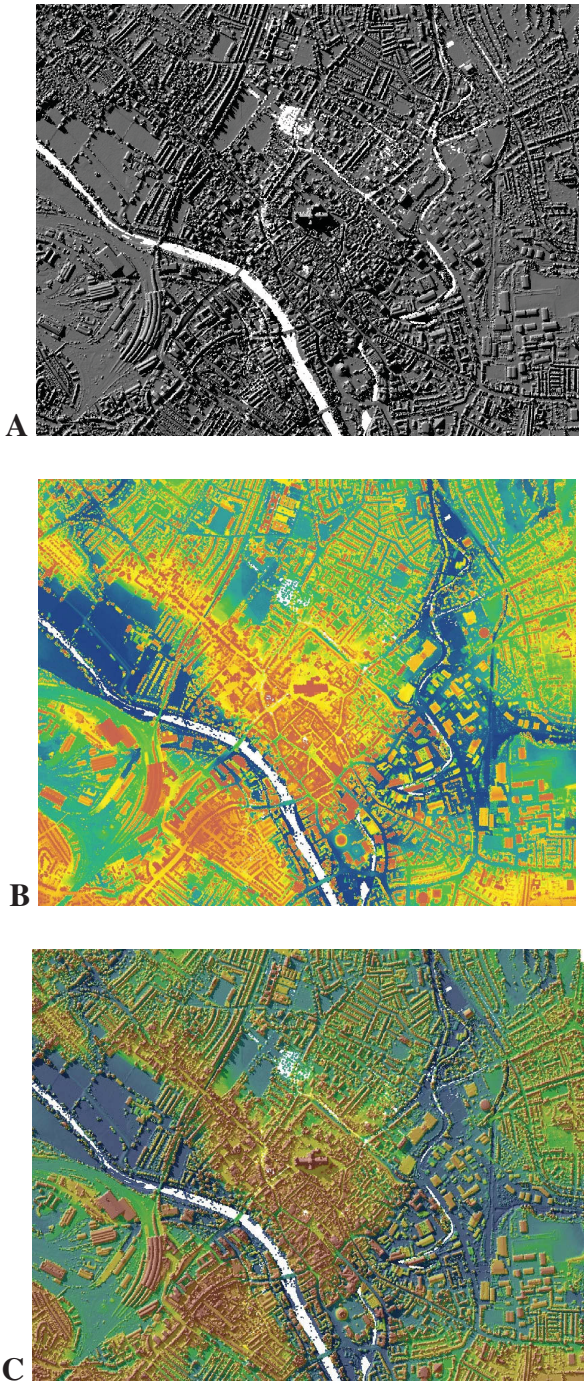

Figure 4. (A) solar-shaded, (B) colour-shaded and (C) combination colour and solar-shaded unfiltered EA LiDAR DSM of York city centre. Even in this difficult terrain, with extensive opaque ground clutter, it is possible to identify subtle aspects of floodplain topography in the carefully shaded surface model.

2.5 Filtering Techniques

LiDAR records the elevation of both the natural land surface and all opaque and semi-opaque objects above that surface. It is often desirable to be able to identify artificial objects standing above the level of the natural land surface, either because those objects are themselves of interest for example to map buildings (Blair *et al* 1999; Priestnall 2000) or land cover (Cobby *et al* 2000). It may also be desirable to produce a model of the bare-earth land surface as a basis for flood modelling, for visualisation applications, or to provide a bare-earth surface as the top of a sub-surface model (*cf* TVG 2002 component 3, Challis 2004).

Separation of elevation values for landscape clutter from those of the underlying bare earth surface requires application of suitable filter to the LiDAR data to identify the values of interest and extract them (Axelsson 1999). If a bare-earth surface model is required then this process must be followed by application of a suitable method of interpolation to fill the resulting holes in the elevation values resulting from removal of landscape clutter.

EA use a variance filter to extract landscape clutter from their DSM data and an undocumented interpolation algorithm to fill holes in the data and produce a DTM. A number of other approaches to filtering DSM data have been documented, for example through the use of artificial neural networks (Jaafar *et al* 1999) or bilinear interpolation (Cobby *et al* 2001).

The present study examines two methods of producing a bare earth DTM from EA DSM data: the use of a high-pass filter to remove landscape clutter and the generation of a simulated first and last-pulse DTM through filtering. In addition the impact of a number of different interpolation methods on DSM data filtered using the EA supplied variance mask were assessed (Figure 5). In each case work was restricted to a single 2x2km LiDAR tile (000416 for a meander core at Gunthorpe in the Trent Valley). The EA data products for this tile are shown in Figure 6 and may be compared with the experimental results.

2.5.1 High-Pass Filter and Interpolation

A McVay 3 x 3 cell high pass convolution filter was used to identify areas of high frequency change in the elevation data. Convolution filters examine every grid cell in turn by application of a moving window. For each grid cell, the cell itself and its neighbours are weighted and multiplied by the corresponding weight (Figure 7). The weighted intensities are summed and divided by the number of cells in the filter window and the calculated value, which replaces the value at the centre of the filter window, written to a new grid. A high pass filter identifies spatially heterogeneous values indicating rapid change in elevation, such data usually correspond with the footprint of buildings, trees, vegetation and other objects standing proud of the gradually changing elevation of the floodplain and terrace surface (Figure 8). Figure 9A shows the effect of applying this filter to the EA DSM; as well as change associated with structures above the floodplain surface the filter has identified high frequency change attributable to interference patterns at the overlap of LiDAR survey swathes. The elevation values extracted by the high-pass filter were reclassified to produce a simple binary filter mask, which was used to remove masked values (high

frequency change) from the DSM. The result (Figure 9B) is a set of elevation values with substantial holes. These holes were filled by interpolation using kriging and a local polynomial function (*infra* section 2.5.3). The kriging interpolation presents a slight visual improvement on that offered by EA, largely as a result of the effects of high-pass filtering in removing the swathe overlap interference. The local polynomial interpolator produces a surface that is too generalised, with some, significant detail of palaeochannels lost in the meander core and with significant interpolation artefacts on the higher slopes at the floodplain edge. Considerable further assessment of the effects of these and other interpolation functions, including comparison with the original elevation values and with elevation values measured (Figure 9E) and in the field, is required before drawing definitive conclusions, but this brief exercise demonstrates that it may be possible to improve on the DTM product supplied by EA, although the time-consuming and computationally intensive nature of such work makes it feasible only for relatively small areas.

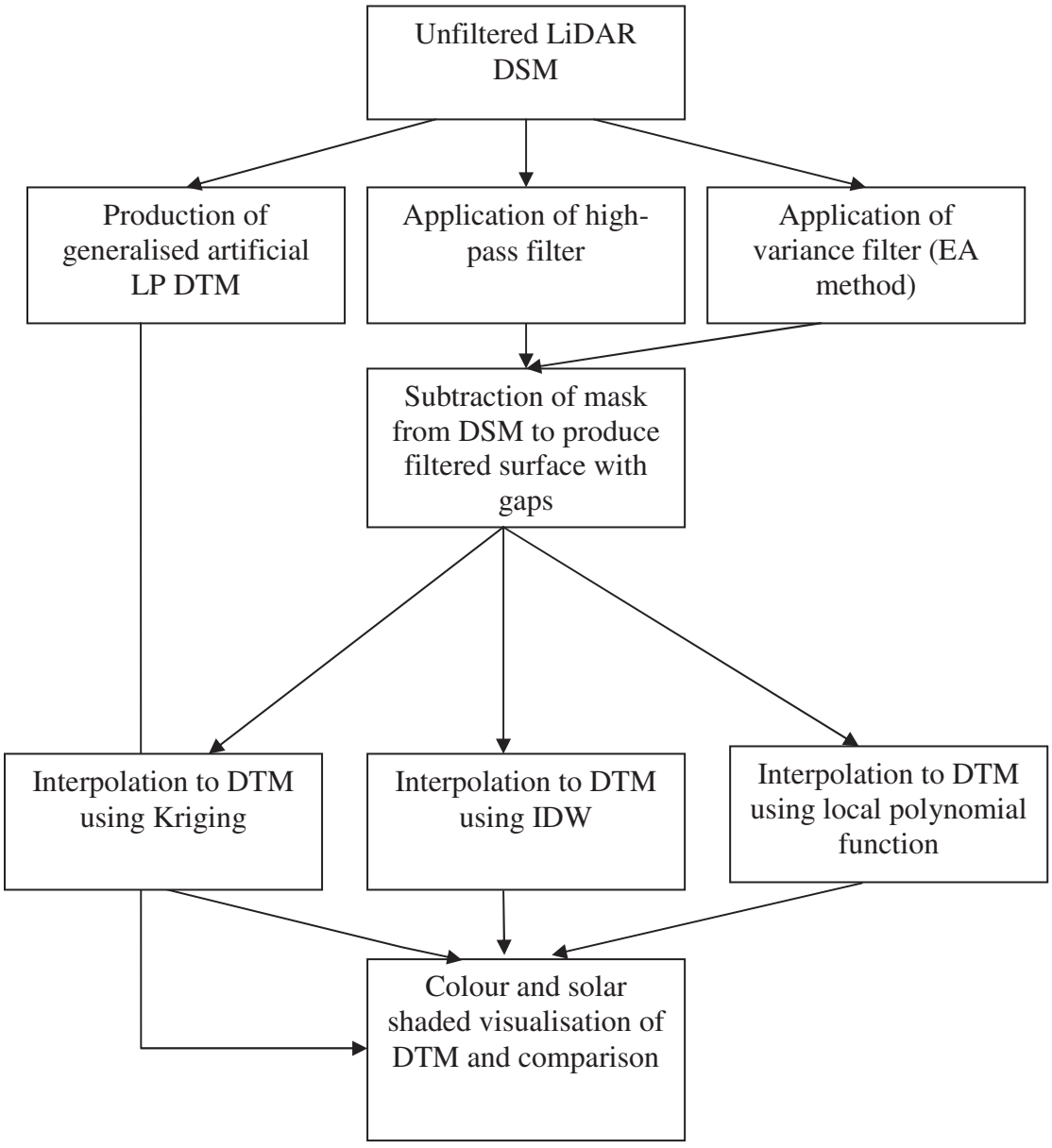

Figure 5. Diagram showing the various trial processes of filtering and interpolation applied to LiDAR data.

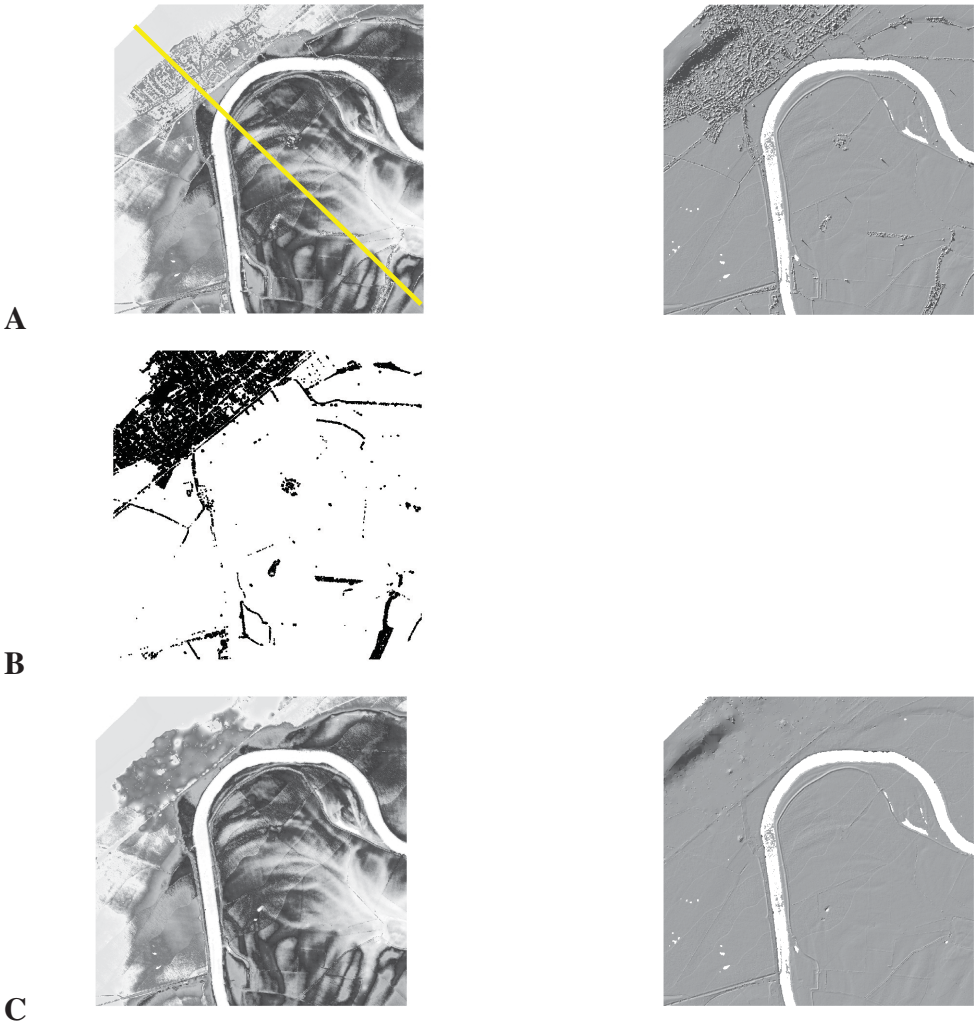

Figure 6. 2x2 km LiDAR tile 0416 showing (A) colour and solar shaded unfiltered EA DSM (B) the EA variance filter mask and (C) colour and solar shaded EA interpolated DTM. The line of the profile in Figures 12 and 14 is shown on A in yellow.

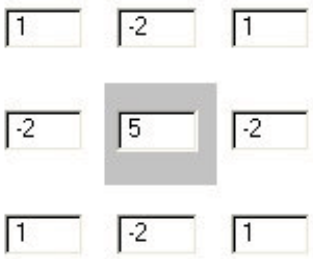

Figure 7. Filter window cell weights for a McVay high pass convolution filter.

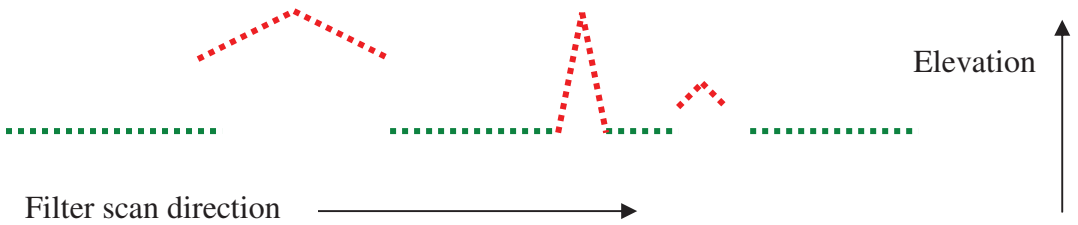

Figure 8. Simulated profile through a LiDAR DSM showing the effect of a high-pass filter. Elevation values representing high-frequency (rapid) change (in red) are extracted from the DSM leaving only those values representing low frequency (gradual) change (in green). The filter is effective as high frequency change usually corresponds to buildings, trees and other opaque and semi-opaque objects on the ground surface.

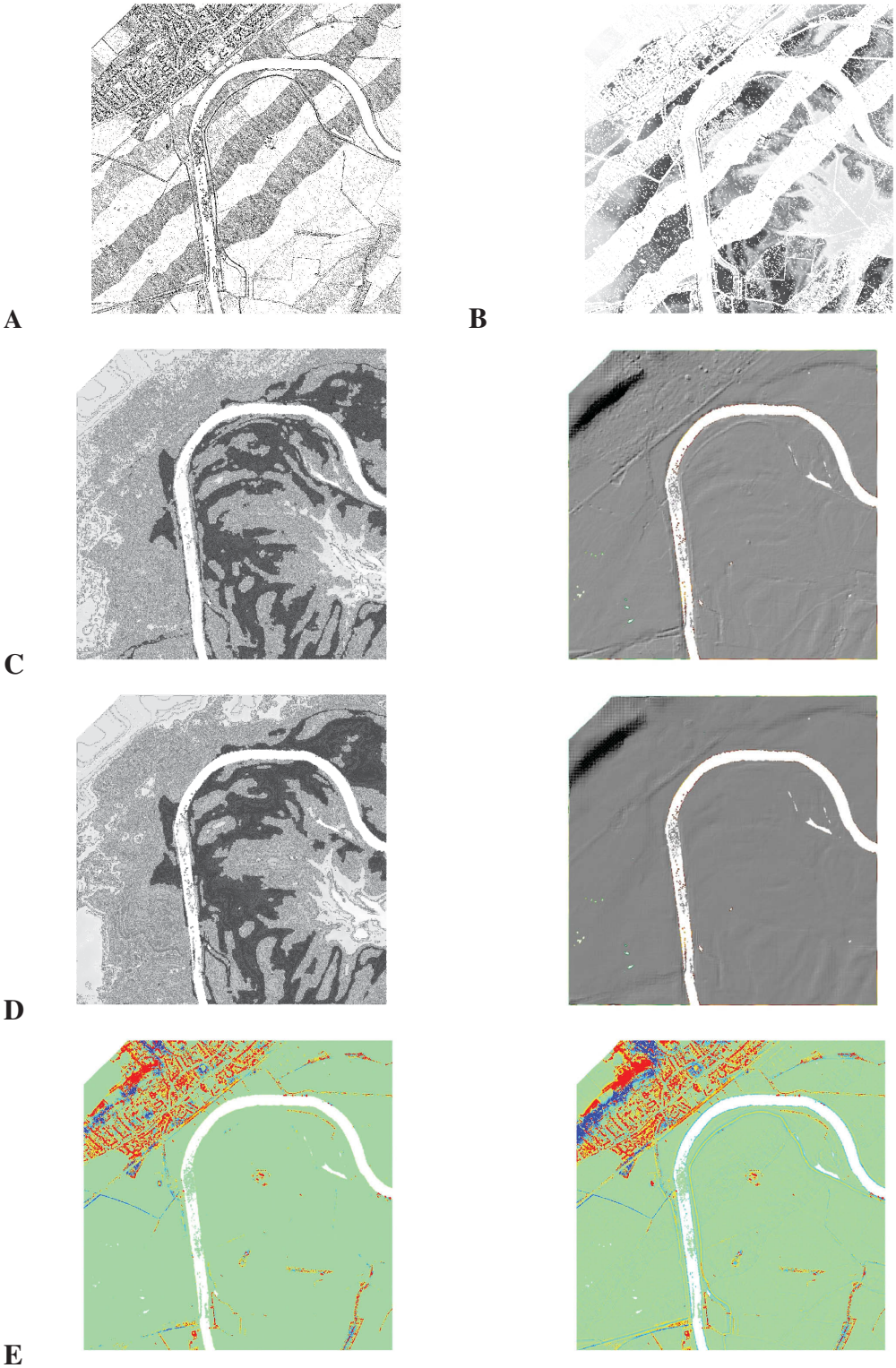

Figure 9. 2x2 km LiDAR tile 0416 showing (A) a high-pass filter mask, (B) the DSM with areas of high-frequency elevation change removed, (C) colour and solar shaded 5m resolution DTM interpolated using kriging ,(D) colour and solar shaded 5m resolution DTM interpolated using a local polynomial function and (E) absolute elevation differences between kriged (left) and local polynomial surfaces (right) and the original EA DSM (red lower than original, blue higher than original, green is no change).

2.5.2 Simulated First and Last-Pulse

EA LiDAR data record only one return of each laser pulse in a single data layer. As has been shown, separation of first and last pulse returns has greater utility. It is possible to simulate this separation from single return data using a grid of coarser resolution that the supplied data if more than one original elevation value falls within each cell of the new grid (Cobby *et al* 2001: 127). Data supplied by EA have a 2m grid resolution. If this data is resampled to a 6m grid resolution each 6m grid cell inherits its value from nine surrounding 2m cells (Figure 10). Within these nine cells the range of heights will vary, typically including values for opaque objects, vegetation and bare earth surfaces together with values beyond the edges of opaque objects smaller than 6m across. As part of this study the original 2m gridded data were resampled to a 6m resolution grid by extracting the highest and lowest original values within each new 6m grid square. The effect is to generate a lower spatial resolution grid with a simulated separation between first pulse (highest elevation value) and last pulse (lowest elevation value) returns (Figure 11).

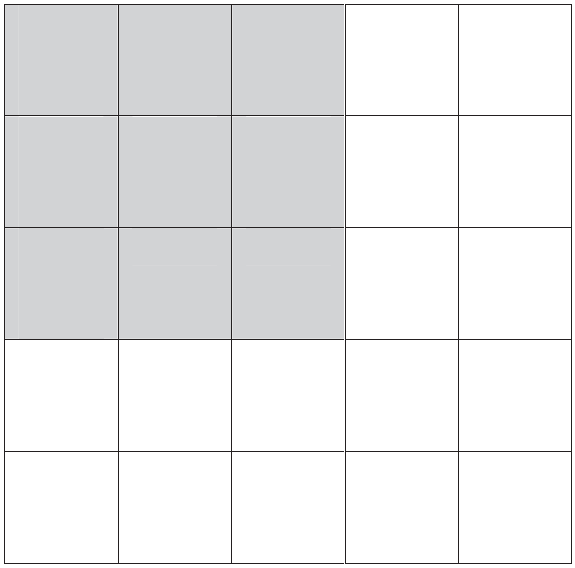

Figure 10. Effect of resampling from a 2m (unshaded) to a 6m grid resolution (shaded). Each 6m grid cell inherits its value from 9 original cells.

This simple, non-computationally intensive, method is remarkably effective at isolating and removing landscape clutter. Opaque objects such as pylons supporting high-voltage power lines, flood banks, buildings and much vegetation are isolated by the extracting the highest elevation values in each 6m grid while use of only the lowest values produces a surface with much of the landscape clutter removed, but with features of the floodplain intact. The difference in elevation between these two DTM, in effect the landscape clutter removed from the simulated last pulse DTM, is shown in Figure 11C.

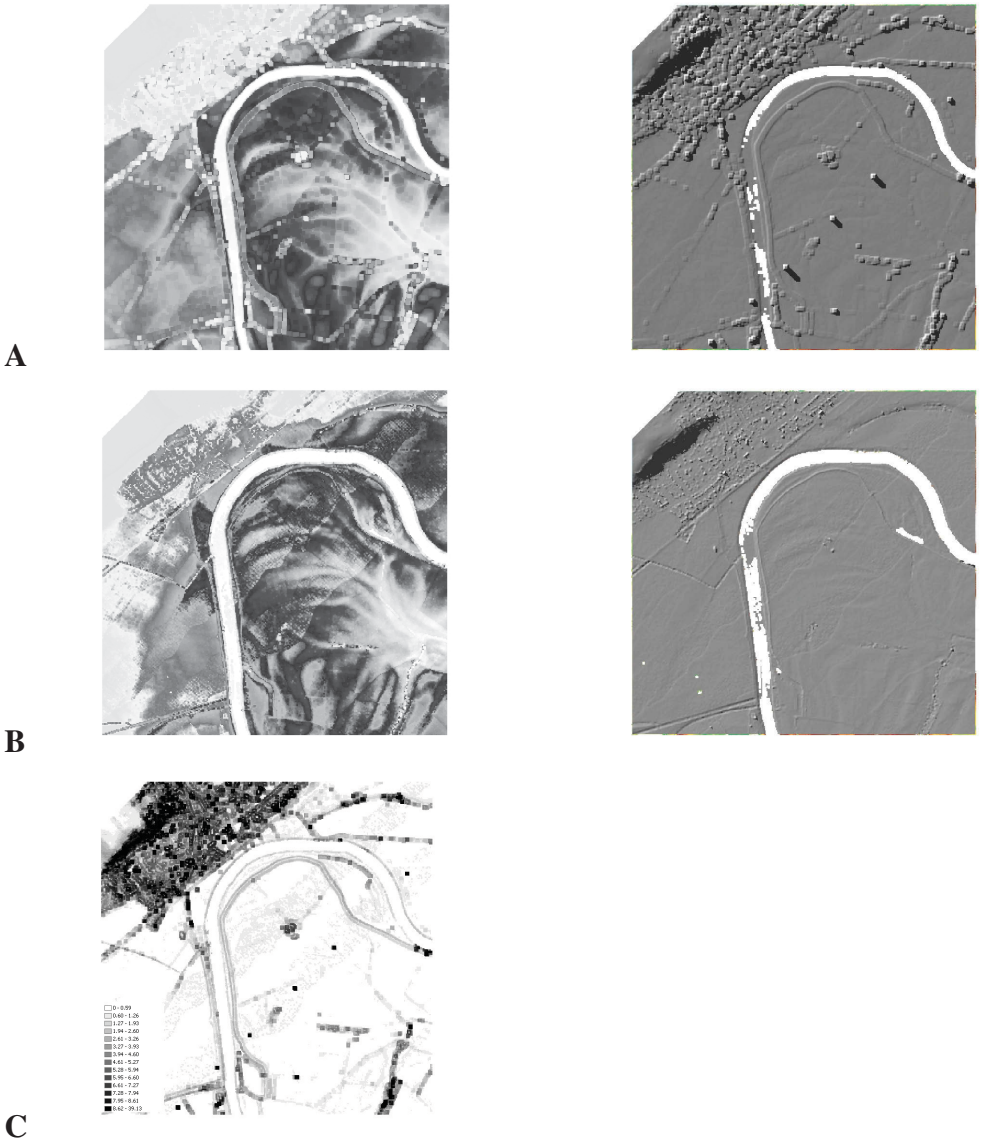

Figure 11. 2x2 km LiDAR tile 0416 showing (A) 6m resolution colour and solar shaded simulated first pulse DTM, (B) 6m resolution colour and solar shaded simulated last pulse DTM and (C) elevation differences between simulated first and last pulse (darker is greater difference).

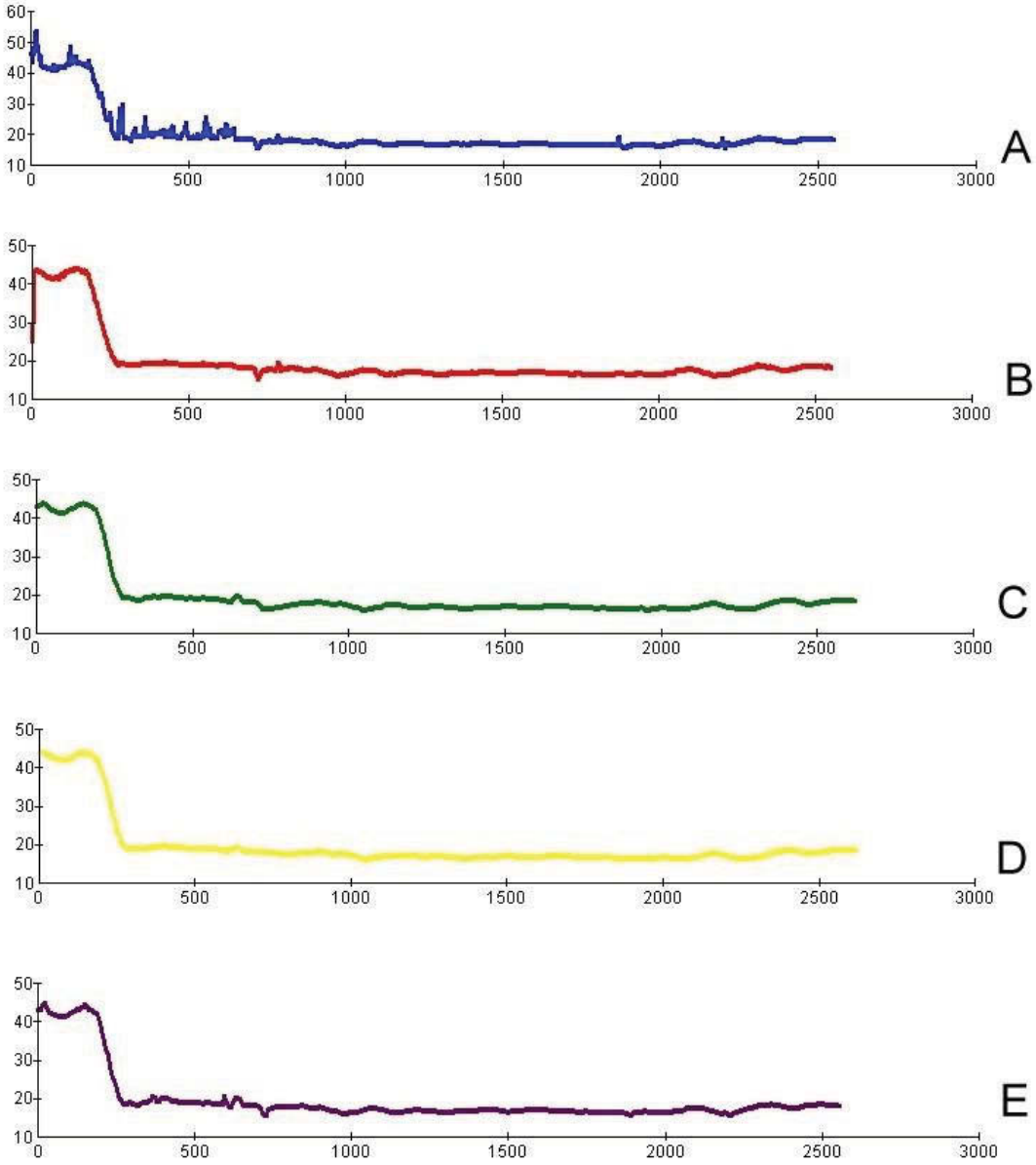

Figure 12. Profiles through LiDAR DSM and DTM. (A) unfiltered DSM, (B) EA filtered and interpolated DTM, (C) high pass filter and kriging, (D) high pass filter and local polynomial interpolation and (E) false last-pulse DTM.

2.5.3 Effects of Different Interpolation Techniques on Variance Filtered DSM

EA supply a filter mask for each 2km tile as part of their standard data product (Figure 13B). In order to test the effectiveness of different interpolation methods on filtered data, the mask was subtracted from the original DSM, leaving a set of elevation values with gaps where masked values were removed. These gaps were filled and new DTM generated using kriging, inverse distance weighting (IDW) and local polynomial interpolation functions. Interpolation was carried out using the Surfer surface modelling package.

Kriging a geostatistical matrix based algorithm, interpolates a smoothed best-fit surface from observations and is widely used in geology and the earth sciences (Oliver and Webster 1990). Its utility in generating LiDAR derived DTM is reviewed by Lloyd and Atkinson (2002). The interpolation function is based on the solution of series of parallel equations modelling the relationship between each grid node, the sample points used in its interpolation, and the interaction between the sample values used for each interpolation. These equations can be controlled to express the spatial characteristics and trends of the sample data where these are known. In particular this allows kriging to model trends between samples so that, for example, high points might be modelled as connected along a ridge, rather than isolated as peaks.

Distance weighting interpolators rely on the assumption that the effect of a given observation on the interpolated surface decreases as a function of the distance from the observation (McCullagh 1988). An inverse distance to a power interpolation function was adopted with a weighting factor of 1 assigned to any sample value that is coincident with a node in the interpolated grid, allowing the incorporation of the values of sample data points faithfully in an interpolated grid. It is a recognised failing of such interpolators that they often fail to model the shape implied by the sample data and can introduce local extrema at the sample points (Mitas and Mitasova 1999).

The local polynomial interpolation method assigns values to grid nodes by using a weighted least squares fit with data within the grid node's search ellipse. For each grid node, the neighbouring data are identified by the user-specified sector search. Using only these identified data, a local polynomial is fit using weighted least squares, and the grid node value is set equal to this value. Local polynomials can be order 1, 2, or 3. The weighted least squares function weights data closer to the grid node higher and data further away lower.

The results of using the three interpolation functions are shown in Figure13, together with profiles through the interpolated DTM. In each case filtering the DSM has removed the majority of landscape clutter. The kriging (Figure 13C) and IDW (Figure 13D) interpolated DTM are largely artefact free and perhaps marginally more effective in the heavily built up areas than the original EA DSM. However, both kriging and IDW display remnants of the marked banding in the original data caused by unresolved survey swath overlaps. The local polynomial interpolator (Figure 13E) has produced a smoothed surface, free of landscape clutter and with the majority of the banding also absent. However, this interpolator has not coped well with the area of steep slope on the north-western edge of the data where substantial artefacts are present.

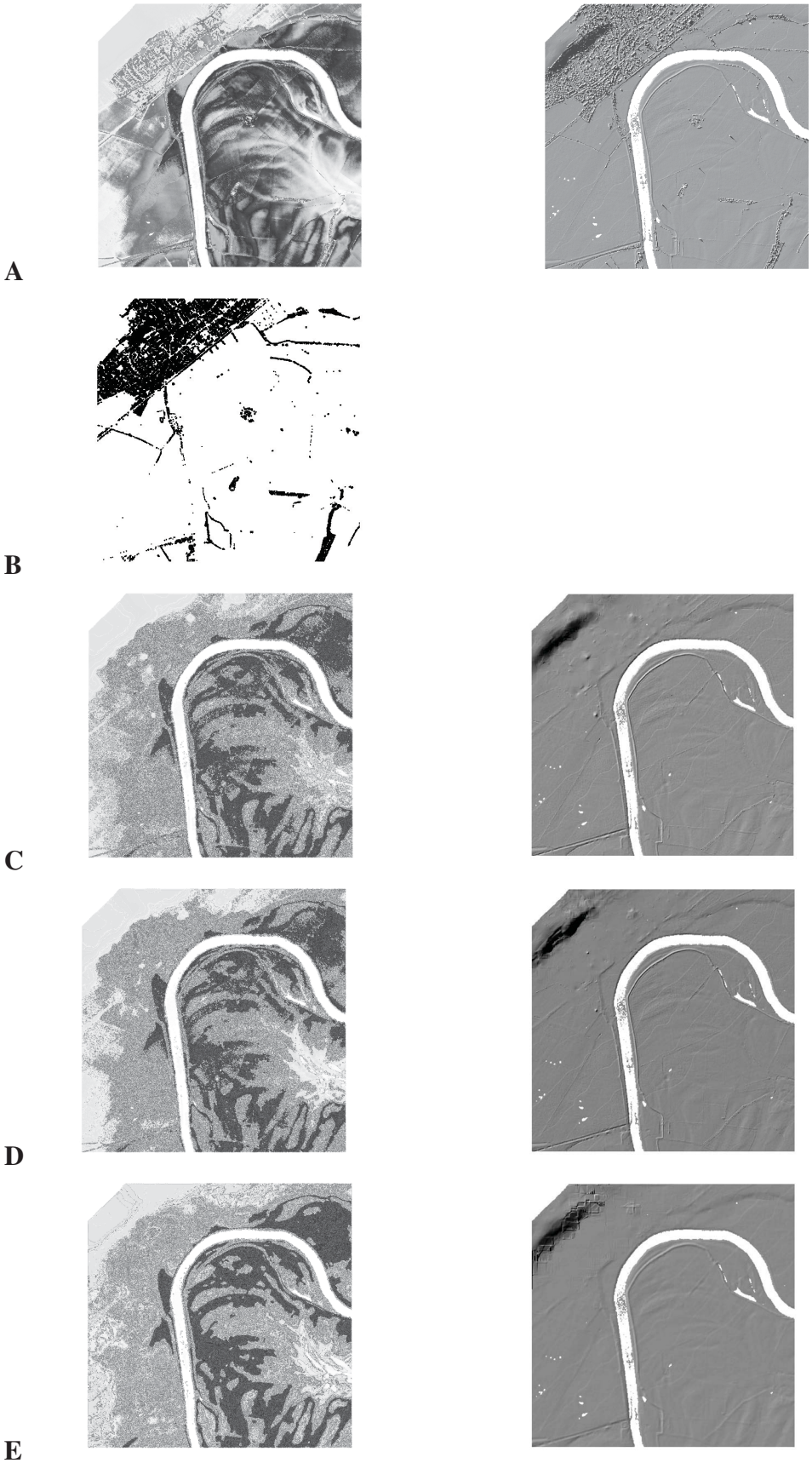

Figure 13. 2x2 km LiDAR tile 0416 showing (A) unfiltered DSM colour and solar shaded (B) the EA filter mask, colour and solar shaded 2m DTM generated using (C) kriging, (D) IDW and (E) a local polynomial function.

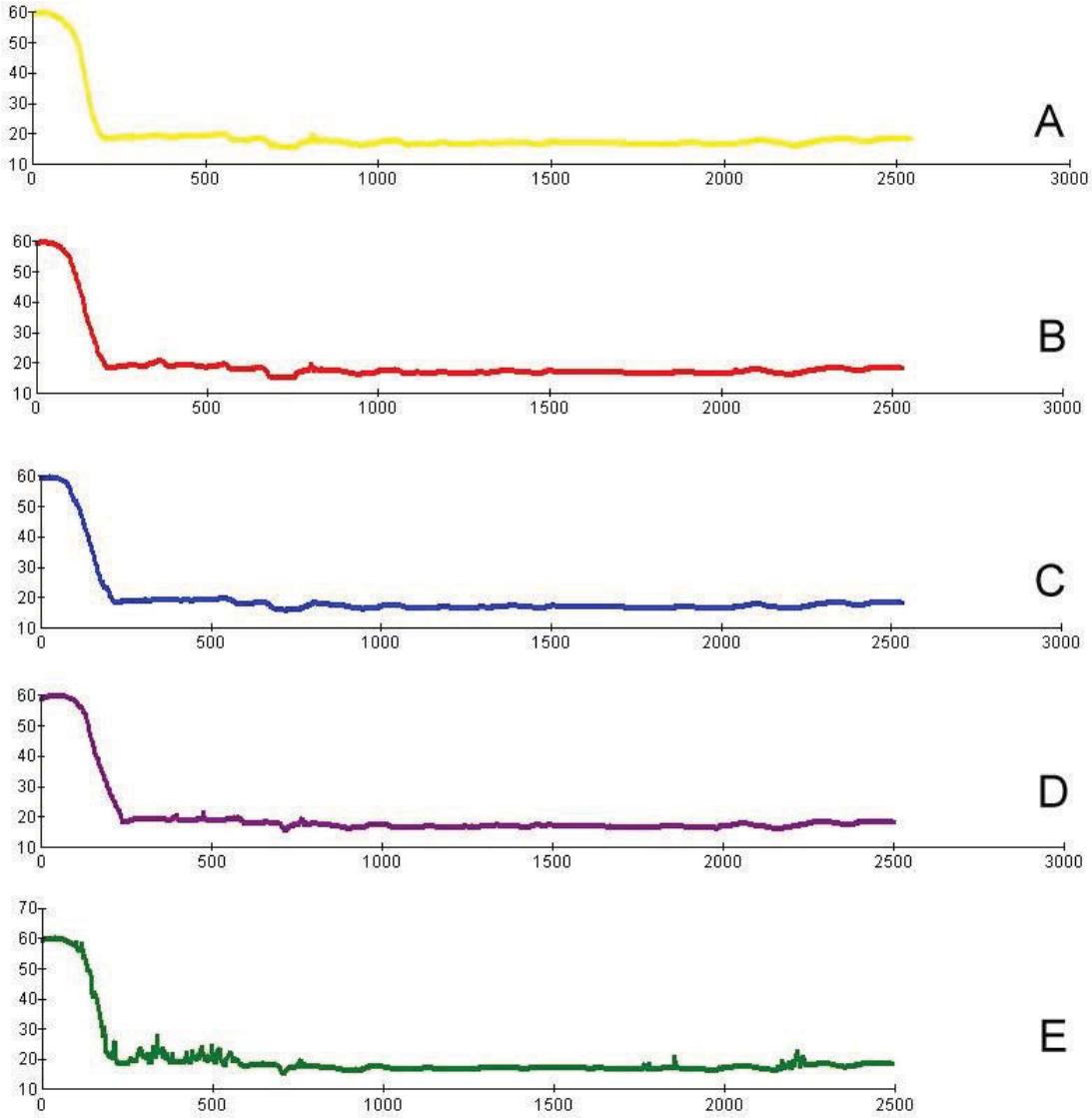

Figure 14. Profiles through LiDAR DSM and DTM. (A) DTM interpolated using IDW, (B) DTM interpolated using kriging, (C)) DTM interpolated using a local polynomial function, (D) EA DTM and (E) unfiltered EA DSM.

2.5.4 Conclusions

In practice it has proven impossible to produce a truly artefact free DTM using the methods trialled. It is clear that for reliable DTM generation access to both FP and LP laser returns is essential (Marks and Bates, 2112), although simulating this with a reduced grid resolution is probably the most straightforward and reliable method of extracting landscape clutter at the cost of a reduction in spatial resolution of the resulting DTM (not necessarily a problem if the DTM is required only for visualisation). Of the other methods tested, data filtered using the EA supplied variance filter mask with gaps filled using a local polynomial interpolator offers the most visually appealing result. Considerable further work is required to test the integrity, accuracy and reliability of this and other interpolated DTM.

Mapping and analysis undertaken as part of this project has used EA DSM, complete with landscape clutter, rather than the EA supplied or any other DTM. The principal reason for using the DSM rather than DTM for archaeological purposes lays in the fact that it is the human-modified landscape, complete with buildings, roads, earthworks, and trees that forms the subject of study. A filtering technique might well identify these features of the archaeological landscape as clutter for removal, thus erasing an essential part of the subject matter of the study.

2.6 Representing Geoarchaeological Features

Part of the intention of the TVG 2002 study was to produce digital data, derived from LiDAR DSM that might be directly compared with exiting data generated by other means, chiefly maps of palaeochannels derived from air-photos as part of component 2A of the project, by Steve Baker of TPAU (Baker 2003).

Such data can be generated either through the intervention of an experienced image interpreter who visually identifies and digitally encodes significant floodplain features, or possibly through an automatic or semi-automatic method whereby an appropriate computer algorithm identifies features of significance based on examination of their digital properties. Both approaches are reviewed below.

2.6.1 User Digitisation

Palaeochannels of the River Trent mapped from air-photographs by Baker are represented using a vector data model, as polygons and polylines with attributes, created by on screen digitising from air-photo mosaics within ArcGIS (Baker 2003).

Similar data have been generated using LiDAR, in effect by treating the colour-shaded LiDAR DSM as an image, with changes in elevation revealing palaeochannels treated in the same manner as crop or soil marks might be on air-photographs. This approach is not wholly satisfactory as continuous raster LiDAR data are able to reveal great complexity of channel form, requiring considerable simplification in order to be captured in a vector data model (see for example Section 3, Figure 28 for an example of complex floodplain geomorphology, compare with Figure 27 as an example of the inadequacies of representing such structures in a vector data format).

In addition vector digitising of the LiDAR data removes one of the key facets of LiDAR that assist in interpretation and visualisation of landscape features: its three-dimensional record of terrain. This has proven particularly useful in identifying and

examining some features of the archaeological landscape such possible round barrows (*infra* section 5 Figures 41-43).

2.6.2 Automatic Feature Extraction

Automatic feature extraction techniques in digital remote sensing usually rely on the varying spectral properties of ground surface materials (i.e. the parts of the electromagnetic spectrum that they absorb and reflect to a varying degree). Using multispectral remote sensing this allows different materials to be isolated by identifying their spectral signature. Techniques based on supervised (with user intervention) or unsupervised (computer only) image classification are commonly used to produce thematic mapping showing soil or rock type, vegetation cover etc. (Mather 1999).

LiDAR imagery provides only variations in elevation (or in the case of some imagery elevation and reflected laser intensity) as a means of identifying features. Automatic feature identification with such data requires the recognition of patterns of change in a single variable, for example to locate the edges of discrete features through rapid changes in elevation or to identify areas of contiguous higher or lower elevation (Axelsson 1999).

A variety of techniques might be employed to achieve this. Priestnall *et al* (2000) used unsupervised classification to identify urban features such as buildings from LiDAR DSM. Haala *et al* (1999) used a combination of mathematical filtering of the DSM and classification techniques combining LiDAR and multispectral imagery to extract building outlines. Cobby *et al* (2003) relied on detrending a LiDAR DSM by subtracting a bilinearly interpolated surface from the original DSM to isolate only those high frequency changes associated with surface texture such as trees and crop height. Rango *et al* (2000) used progressive detreding of a LiDAR DSM to identify areas of high frequency elevation change representing sand dunes.

The above examples rely on relatively dramatic high frequency changes in elevation to identify sharp edges of discrete features such as houses, or broad areas of differing elevation such as woodland. Channel features on floodplains present a greater challenge as they are sinuous rather than straight sided, often have gradual rather than sharply defined edges and may encompass areas of both lower and higher elevations than surrounding land.

In an exercise in broadly similar challenges Lohani and Mason (2001) employed adaptive height thresholding to locate tidal channel fragments in LiDAR DSM of tidal flats and saltmarshes. This technique relies on grouping of similar pixel values in a one-bit (binary) image derived from the LiDAR DSM. This approach has been tested on LiDAR data from the Trent and Witham Valleys. Figure 15A shows the DSM for a part of the Witham Valley where roddens and creek ridges, slightly raised sinuous relict channels revealed by peat shrinkage (Goudie 1990, 310 and figure 9.5) define a prehistoric drainage system. Here, the floodplain floor is almost level, with little underlying elevation trend in the data. A rectilinear pattern of modern field boundaries is superimposed on the sinuous relict channels. Figure 15B shows a thresholded version of the LiDAR DSM. The pattern of relict channels is clearly revealed as distinct from the landscape background, however, some modern landscape

clutter remains. The channels are relatively easily extracted from this image by selecting only the pixel values for the channel features. The overall result would be improved by initial filtering to remove modern landscape features before thresholding.

Figure 16A shows a meander core at Gunthorpe in the Trent Valley, complete with ridge and swale and flood thalwegs, in this case represented by slight depressions in the largely level floodplain. Thresholding of the image (Figure 16B) succeeds in isolating some of the channel features, but the very slight changes in elevation revealing minor channels, together with slight changes in underlying elevation of the floodplain, mean that this technique is not wholly successful in isolating channels. Initial detrending of the data and filtering to remove modern landscape clutter may improve the results.

2.6.3 Conclusions

Automatic feature extraction techniques, although showing some potential, have proven too problematic to be reliable. In general the experience of Barnes (2003) who concluded that the human eye was better than automated systems for detecting the subtle changes (in LiDAR and other remotely sensed imagery) that characterise features of the archaeological landscape must be echoed.

In addition, the difficulties is summarising continuous raster data in a discrete vector format must be emphasised. The vector data derived from the LiDAR through manual image interpretation should be seen as a summary of the detailed representation of landscape captured by LiDAR, suitable for incorporation in a risk-mapping or asset management GIS, but requiring access to the original raster LiDAR data for detailed analysis or threat assessment.

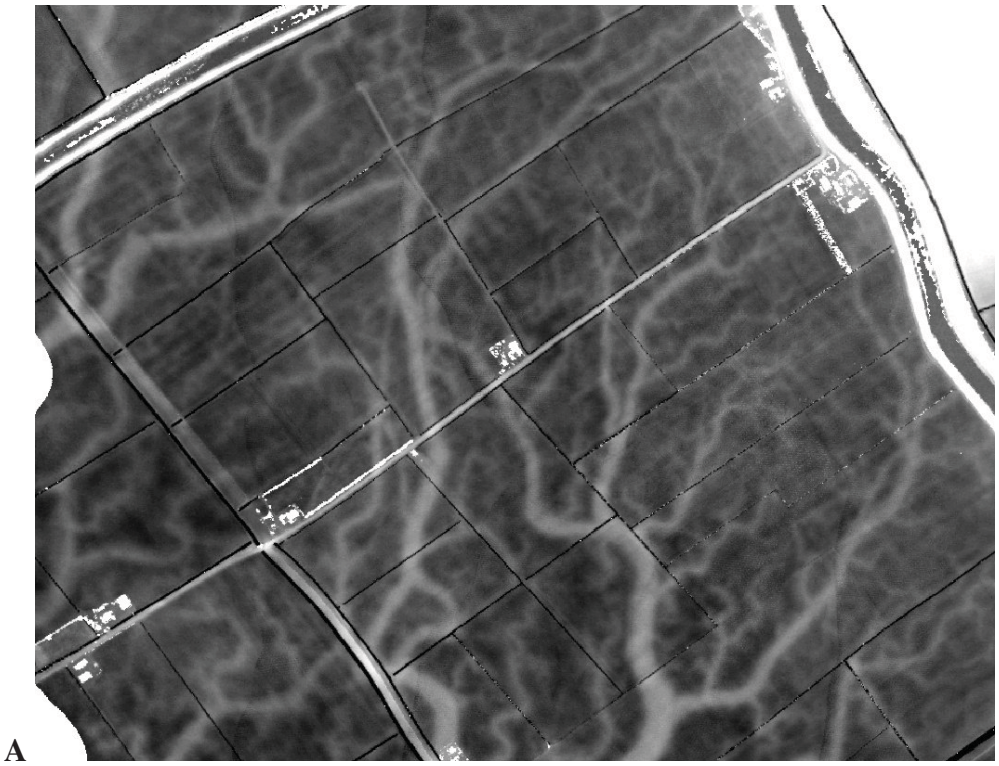

A

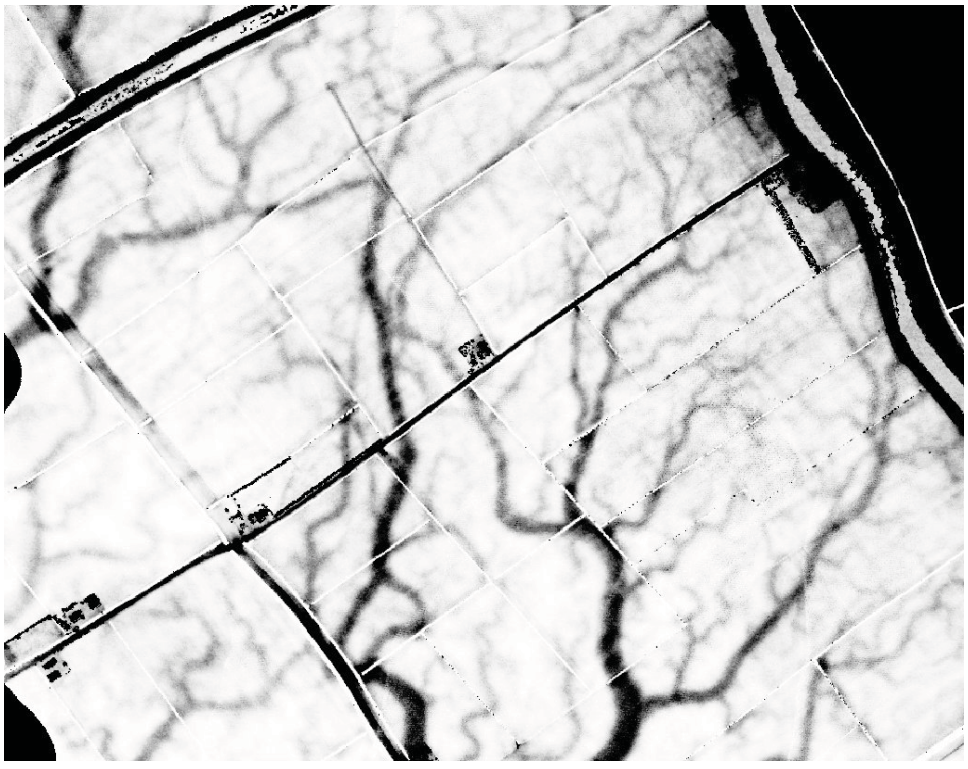

B

Figure 15. (A) LiDAR DSM of a part of the Witham Valley in Lincolnshire showing sinuous relict channels as raised roddens and creek ridges. (B) the same data threshold ed. The majority of the relict channels are isolated by this method, and are relatively easily extracted automatically, however, some modern landscape detail remains.

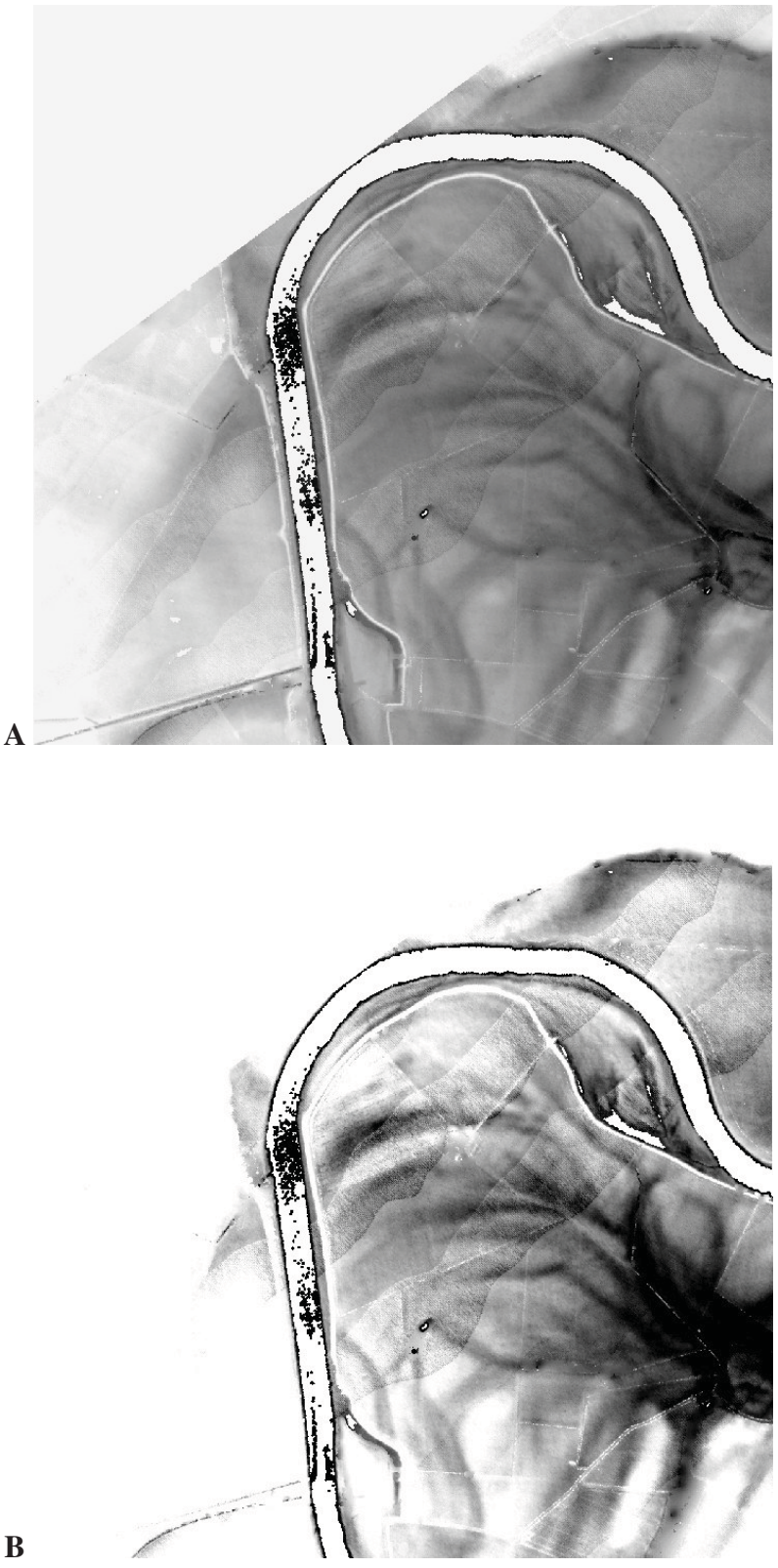

Figure 16. (A) LiDAR DSM showing ridge and Swale and flood thalwegs within meander core of the Trent at Gonalston, Nottinghamshire. In this case the relict channels are defined by slight depressions in the surface. (B) thresholded view of the same data, the relict channels are more clearly defined, but still elude automatic extraction.

3 THE RIVER TRENT

3.1 Introduction

The River Trent rises on the Staffordshire moorlands flowing east and north to join the Humber Estuary at Trent Falls. The Trent varies considerably in character throughout its 250km length. Upstream of Alrewas in Staffordshire the valley is narrow and the floodplain of limited width. Downstream of Alrewas the valley widens and the contemporary channel increases in sinuosity, with frequent palaeochannels on a broad floodplain. Downstream of Cromwell Lock in Nottinghamshire the Trent is tidal and beyond the Idle the Trent is perimarine in character, with subdued topography and substantial depths of peat and alluvium accumulated across a broad valley floor. These differing river reaches display many of the varying characteristics of lowland British rivers described by Howard and Macklin (1999) this makes the Trent an ideal case study for investigating the use of LiDAR for geoarchaeological prospection in a variety of alluviated landscapes.

In common with other Midland rivers the Trent has changed in character throughout the Holocene (Brown *et al* 1994) developing from a Late Glacial and Flandrian braided system to a stable multi-channel anastomosing system and to the present stable single channel. Aspects of these stages of Holocene river development are preserved as topographical features in the floodplain and terraces of the Trent, especially in its middle reaches.

LiDAR coverage for the Trent Valley is limited, but the data available from EA allowed the investigation of river reaches in the upper, middle and lower Trent.

3.2 The Upper Trent Valley

In the Upper Trent Valley LiDAR data were available for a 25km reach stretching from the confluence of the Trent with the River Sow at Great Haywood, upstream as far as Trentham Gardens, Stoke on Trent In this reach the valley is narrow and the Trent is characteristic of a high-energy river system (Howard and Macklin 1999) with coarse-grained sedimentation dominant and with limited fine-grained sedimentation.

LiDAR for this river reach is effective for visualising the general topography and structure of the Valley. However, few palaeochannels or other floodplain features were evident, neither were such features noted by the palaeochannel mapping based on aerial photography undertaken as component 2A of TVG 2002 (Baker 2003).

A few palaeochannel are apparent on the broader floodplain of the Trent at its confluence with the River Sow, where they are evidenced by slight depressions in the floodplain surface (Figure 17). The most substantial of these channels has been investigated with a core sample to examine stratigraphy (as part of component 11a of TVG 2002; Havelock and Howard 2004).

The relative scarcity of palaeochannels is confirmed both by LiDAR and aerial photography. This is a reflection of the narrow valley floor and high river gradient which means that palaeochannels and other palaeo-floodplain features are rarely

preserved, suggesting that the geoarchaeological potential of much of this river reach is relatively low.

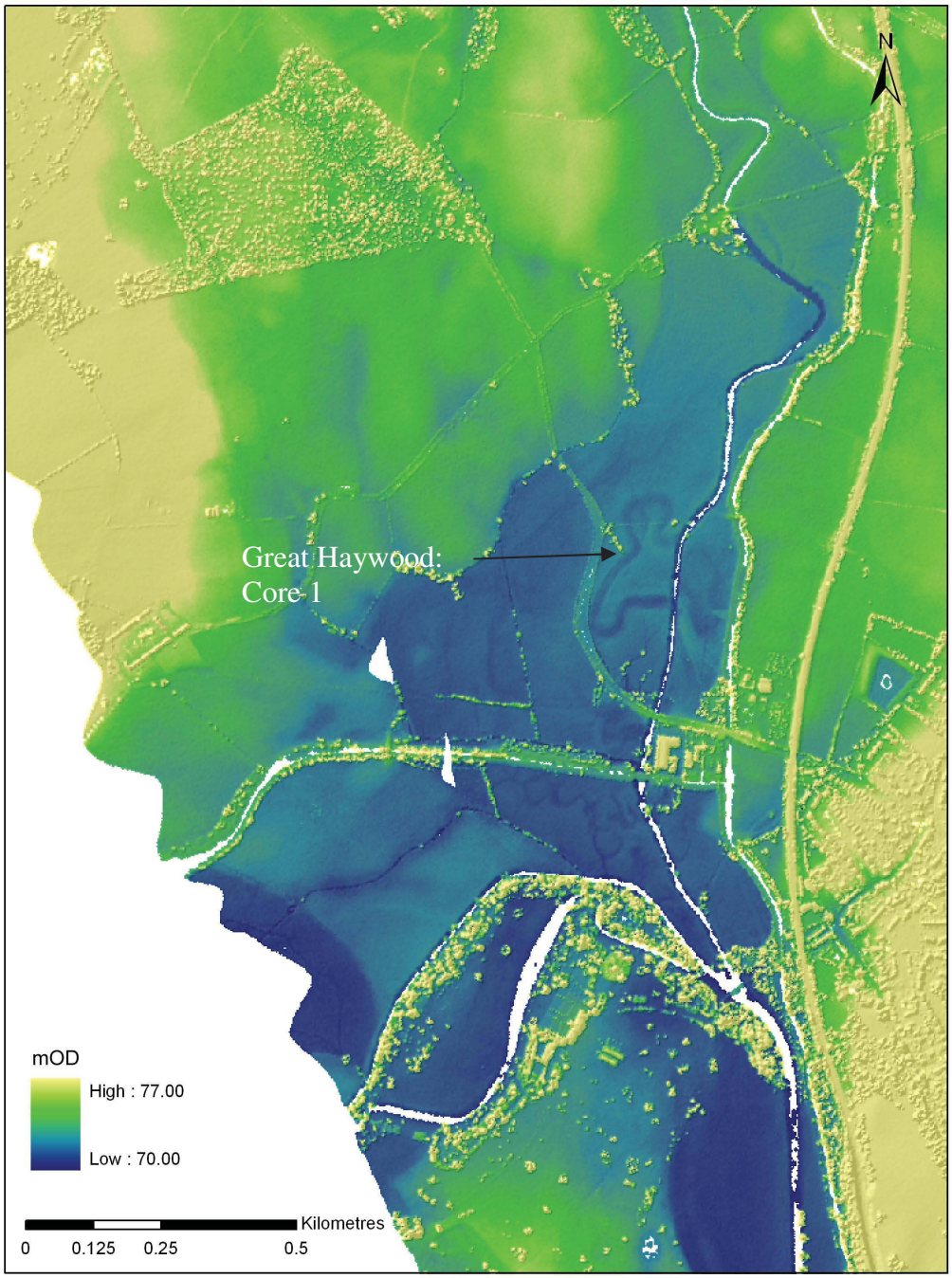

Figure 17. Colour-shaded LiDAR DSM of the Upper Trent Valley at Great Heywood showing details of palaeochannels within the floodplain and the location of core sample 1 taken by Havelock and Howard.

3.3 The Middle Trent Valley

In the Middle Trent Valley LiDAR were available for two substantial and contrasting areas; a 18km stretch of the Derbyshire Trent Valley between the confluence of the Trent with the Rivers Dove and Derwent and in Nottinghamshire a 11km portion of the Trent lying within the Trent Trench and centred on Gunthorpe.

3.3.1 Derbyshire

LiDAR data for the Trent Valley in Derbyshire covers an 18km length of the Middle Trent Valley from the upstream confluence with the River Dove at Doverbridge to the downstream confluence with the River Derwent at Great Wilne (Figures 18 and 19).

The drift geology of this reach has recently been remapped by British Geological Survey (Loughborough Sheet 141; Carney *et al* 2002) providing a very detailed interpretation of the floodplain and terraces against which the LiDAR may be compared (Figures 20 and 21). The chief components of the drift geology are the older Beeston and Hemington Terrace deposits and the younger Holme Pierrepont Sand and Gravel deposits. The floodplain encompasses a number of abandoned and active channel belts, suggesting a past anastomosing river regime. The LiDAR DSM reveals extensive geomorphological detail of the floodplain and terraces, including topographic detail of the terrace surfaces suggesting relict braid channels, together with ridge and swale and extensive detail of past channel activity across both terraces and floodplain. Such detailed information facilitates rapid geomorphological mapping and the assessment of potential for survival of both cultural and palaeoecological archaeological material, assisting for example in the compilation of risk maps such as those developed as part of component NN of TVG 2002. Coring and dating of palaeochannels of the Trent identified through use of the LiDAR DSM (Figure 21) at Repton (Old Trent Water, Core 3) and Twyford (Mill Plantation, Core 4) has been carried out by Havelock and Howard (2004) as part of component 11a of TVG 2002.

The extensive LiDAR coverage of this reach has allowed detailed comparison of the extent to which palaeochannel information plotted from conventional air-photographs (Figure 22: by Steve Baker of TPAU as part of Component 2A of TVG 2002) may be supplemented by LiDAR (Figure 23). In general in areas of high-quality air-photo coverage (such as this) the record of palaeochannels produced is impressively complete and the majority of features identifiable as palaeochannel on the LiDAR DSM are also recorded by mapping from air-photographs. The main additional contribution made by access to the LiDAR DSM is resolution of fine details of geomorphology of the terrace and floodplain, assisting in interpretation of features of uncertain origin or authenticity (a difficulty noted by Baker 2003) and access to three-dimensional elevation data, for example to produce cross-channel profiles.

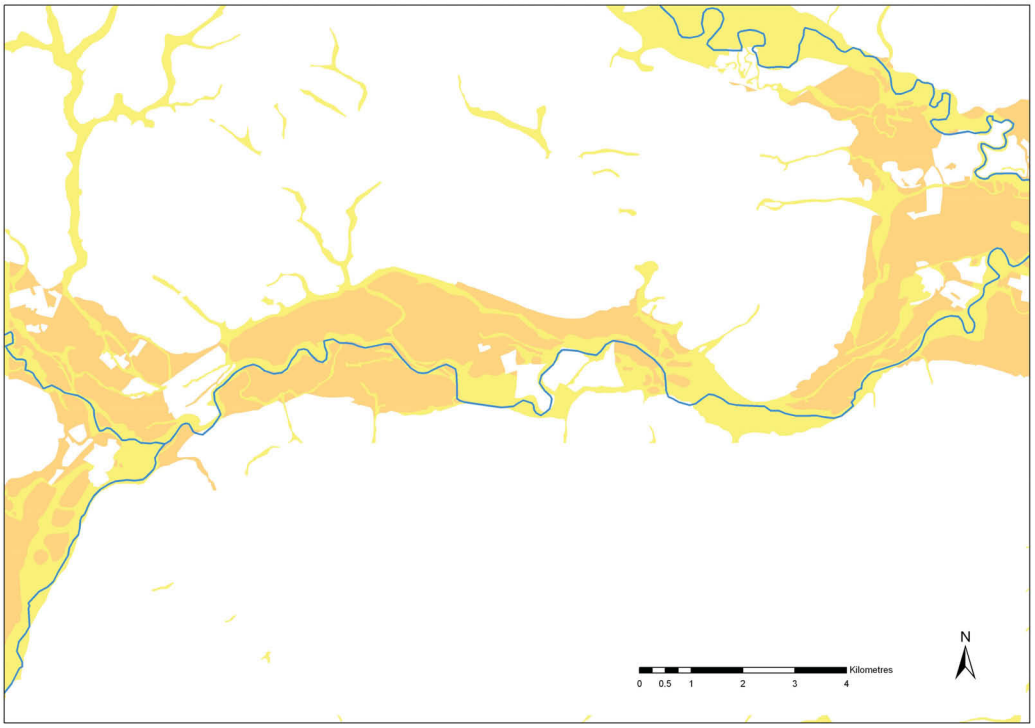

Figure 18. Map showing the floodplain (yellow) and terraces (brown) of the Middle Trent Valley between the Rivers Dove and Derwent.

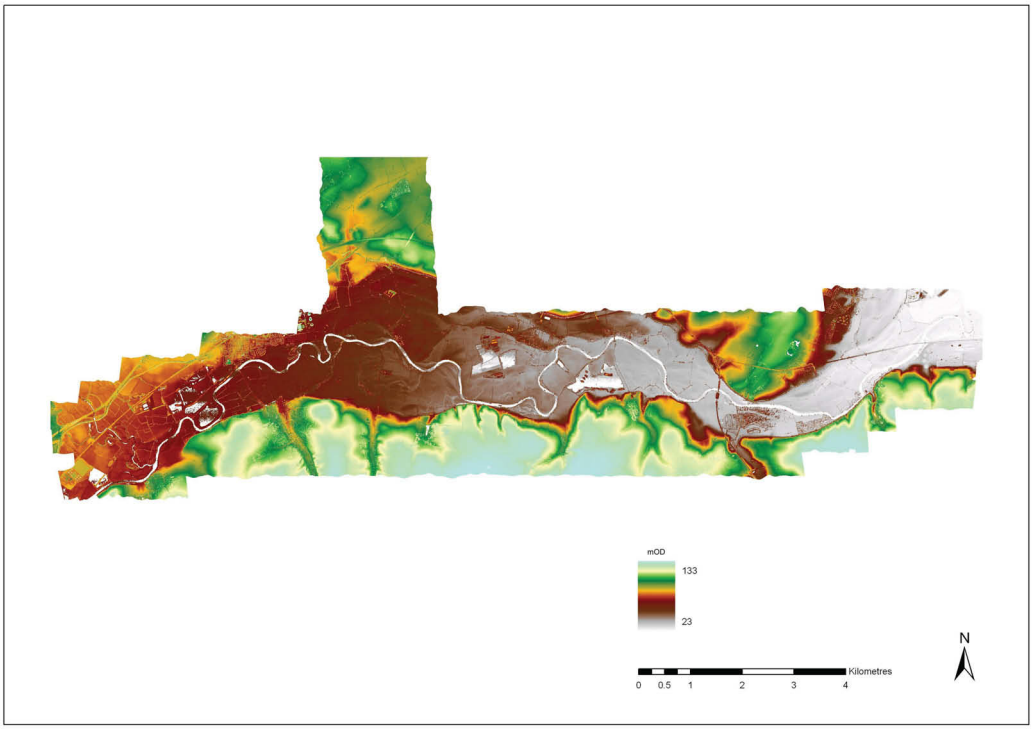

Figure 19. Colour-shaded LiDAR DSM of the Middle Trent Valley between the Rivers Dove and Derwent.

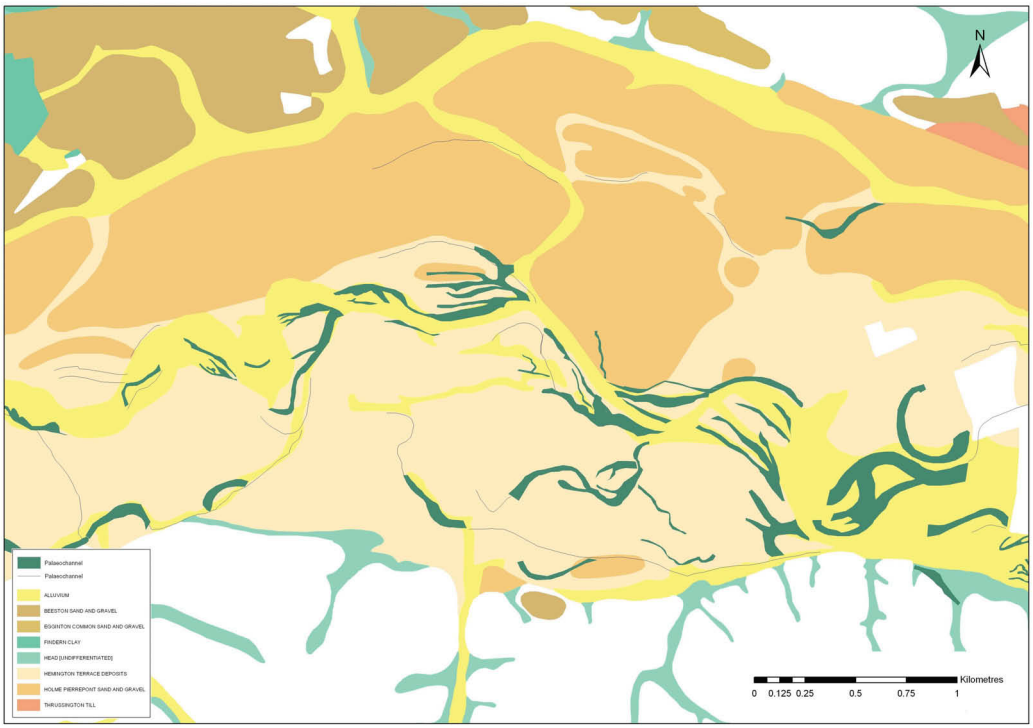

Figure 20. The Middle Trent Valley centred on Twyford, Derbyshire showing the Geological Survey mapping of the drift geology of the terraces and floodplain with palaeochannels mapped from air-photos superimposed.

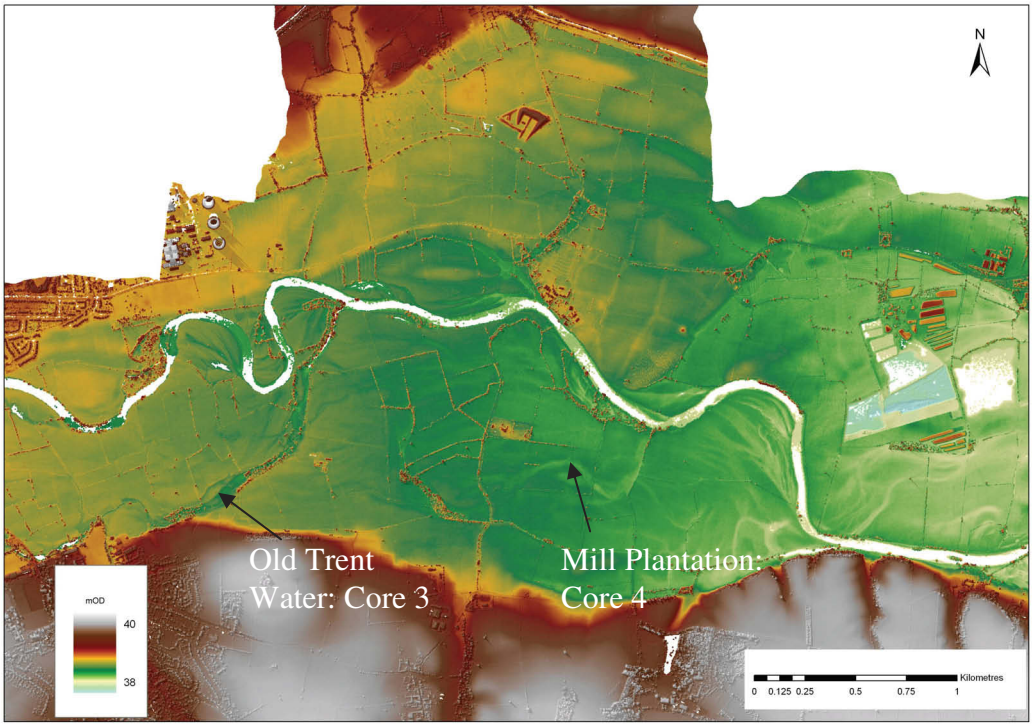

Figure 21. Colour-shaded LiDAR DSM of the area shown in Figure 20. The principal units of the drift geology are clearly evident, as is a mass of additional detail of the geomorphology of the terraces and floodplain. The Locations of core samples of palaeochannels taken by Havelock and Howard are shown.

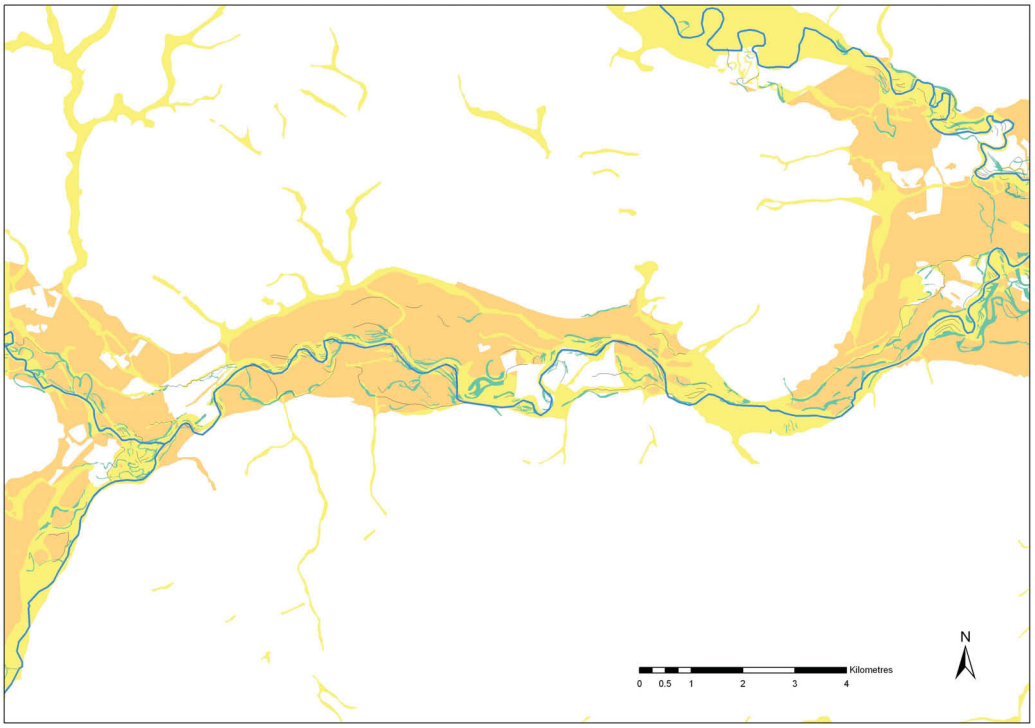

Figure 22. Map showing the floodplain and terraces of the Middle Trent Valley between the Rivers Dove and Derwent with the locations of palaeochannels plotted from air-photographs shown in grey.

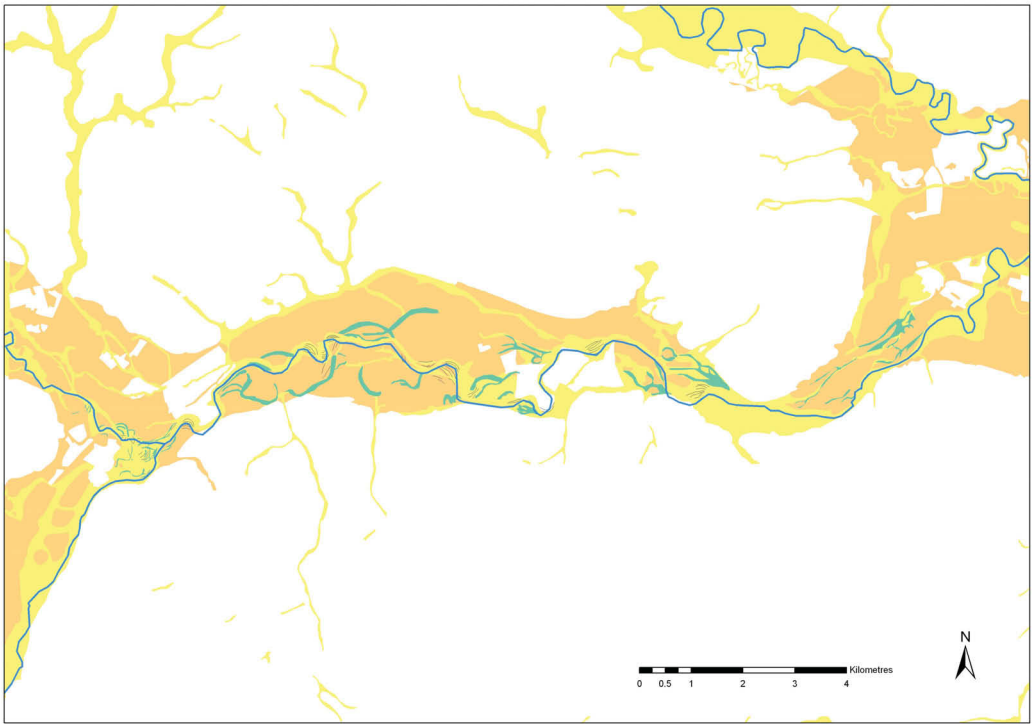

Figure 23. Map showing the floodplain and terraces of the Middle Trent Valley between the Rivers Dove and Derwent with the locations of palaeochannels plotted from LiDAR data shown in grey.

3.3.2 Nottinghamshire

LiDAR for the Middle Trent valley in Nottinghamshire was selected to provide coverage for a 11km stretch of the Valley from Carlton downstream to Hoveringham, centred on Gunthorpe.

Once again, the geology of this reach has been recently remapped by British Geological Survey (Nottingham Sheet 126) providing a detailed understanding of the drift geology (Figure 24) to which the LiDAR DSM (Figure 25) may be compared. The geology of the terrace and floodplain is relatively straightforward in this reach, with terrace materials represented by the Holme Pierrepont Sand and Gravel and the silts and clays of the floodplain indicating a number of principal channel belts including that occupied by the present stable single channel of the Trent.

Valley sides are framed by relatively steeply rising hills, as the Trent in this reach cuts obliquely across the dipslope of the Triassic Mercia Mudstone in a 3-4km wide trench, the Trent Trench, formed as a result of glacially impeded drainage (Dugdale 1988; Straw 2002).

A further comparison of the use of LiDAR in mapping palaeochannel was made, in this instance with palaeochannels mapped from air-photographs as part of a pilot study undertaken by TPAU in 1998 (Garton and Malone 1998). Difficulties were encountered in mapping channel in this area both due to the scarcity of high-quality air-photographic evidence and because of the complexity of features within the floodplain.

The record of palaeochannels mapped from air-photographs (Figure 26) is clearly incomplete, with fragmentary features, clearly parts of larger palaeochannels, mapped in many places. In this reach access to the LiDAR DSM has substantially increased the completeness of the record of palaeochannels (Figure 27). The LiDAR DSM also provides a record of the fine details of some particular aspects of floodplain development. This includes a sinuous former channel of the Trent at Gunthorpe, investigated by coring as part of Component 11a of TVG (Havelock and Howard 2004) and complex area of ridge and swale probably supplemented by flood thalwegs within the core of a meander (Figure 28). A substantial flat-bottomed trough between Caythorpe and Gunthorpe and followed by the line of Car Dyke probable represents a former course of the Trent (Figure 29) while to the north-east the complexity of clay and silt filled former channel may represent the vestiges of an early Holocene braid-plain with a veneer of later alluvium.

It is worth noting that complex and subtle geomorphological features such as these defy easy representation as vector digital data; this highlights the problematic nature of any record of floodplain and terrace geoarchaeology stored in vector format and the need for continued access to both the raster LiDAR DSM and digitised and georeferenced air-photographs as an aid to interpretation and decision making.

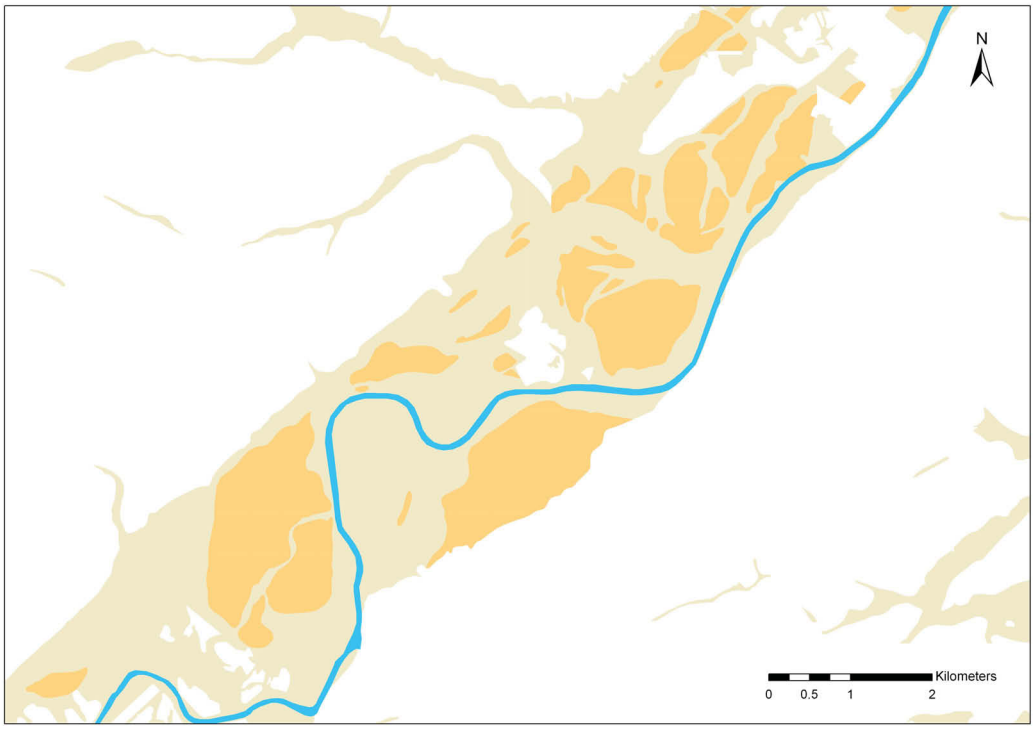

Figure 24. Map showing the floodplain (yellow) and terraces (brown) of the Middle Trent Valley at Gunthorpe.

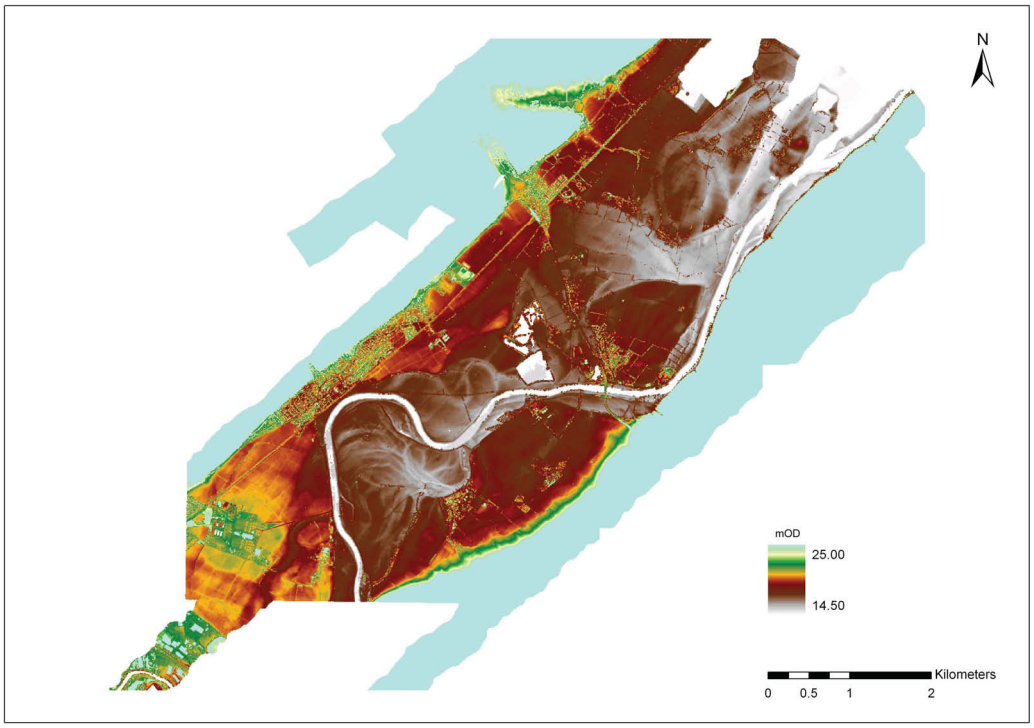

Figure 25. Colour-shaded LiDAR DSM of the Middle Trent at Gunthorpe. The complex geomorphology of the floodplain and terraces is clearly evident.

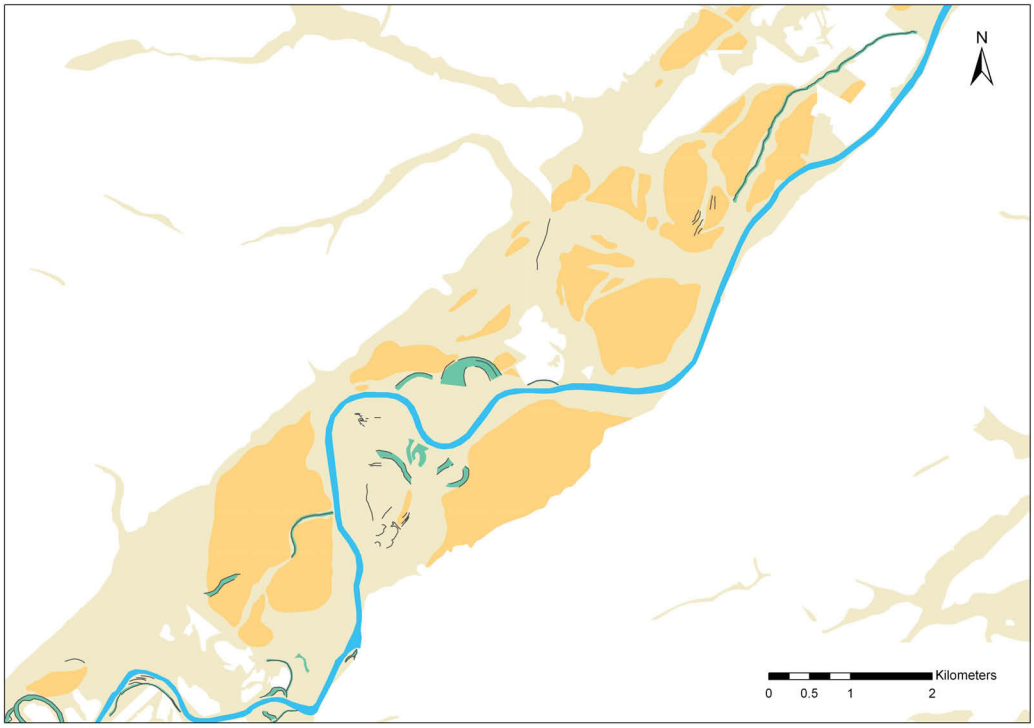

Figure 26. Map showing the floodplain and terraces of the Middle Trent valley at Gunthorpe with the locations of palaeochannels plotted from air-photographs shown in grey.

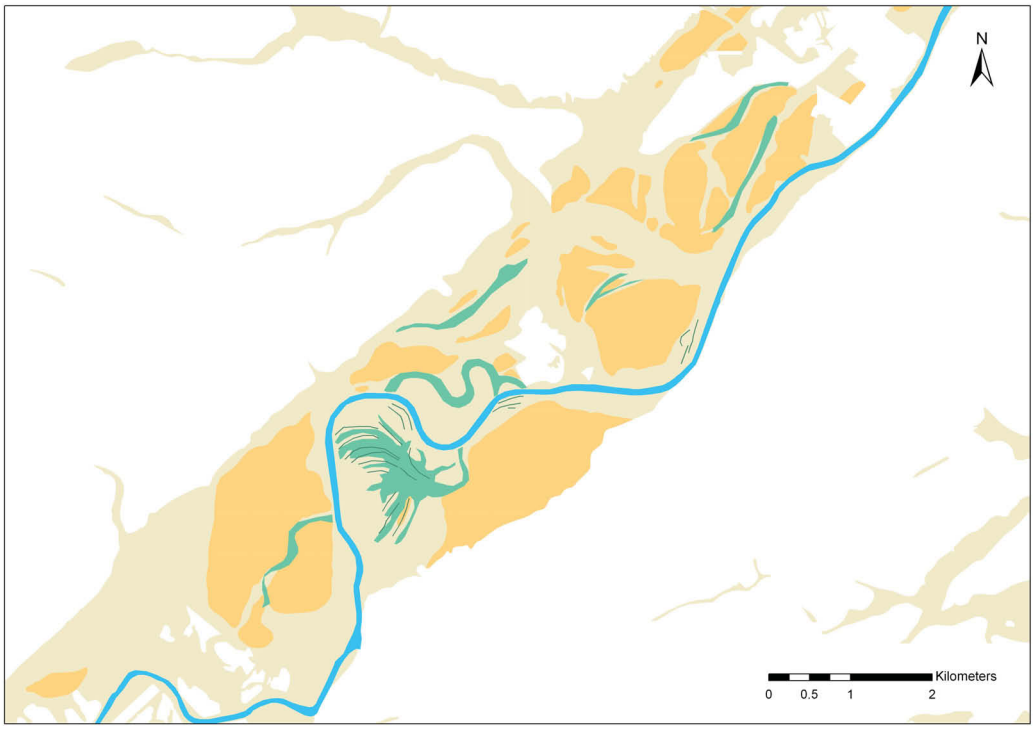

Figure 27. Map showing the floodplain and terraces of the Middle Trent valley at Gunthorpe with the locations of palaeochannels plotted LiDAR data shown in grey.

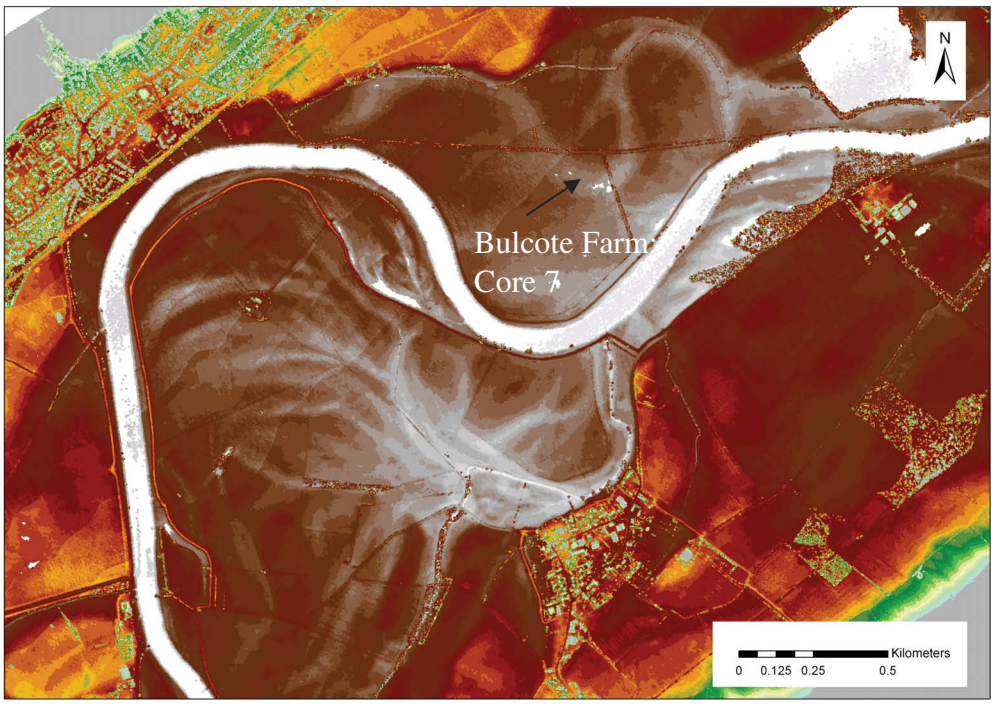

Figure 28. Colour-shaded DSM of the Middle Trent Valley at Gunthorpe showing sinuous palaeochannel of the Trent and a complex arrangement of ridge and swale and probable flood thalwegs within a meander core. The location of core sample 7 taken by Havelock and Howard is also shown.

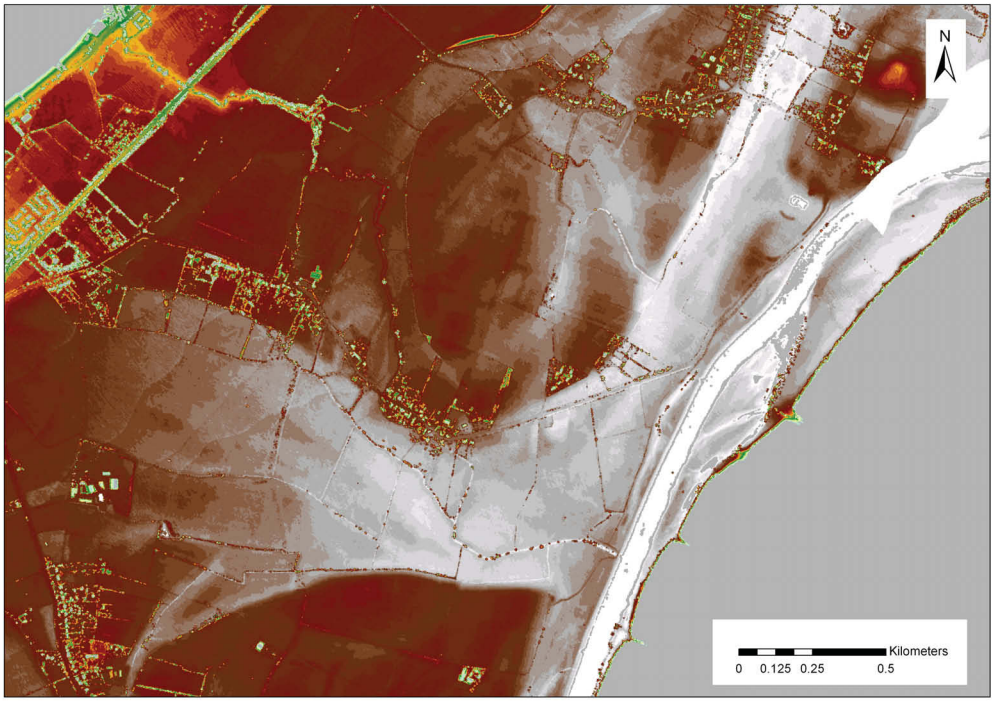

Figure 29. Colour-shaded DSM of the Middle Trent Valley at between Caythorpe and Gunthorpe showing a substantial flat-bottom trough now followed by Car Dyke, but perhaps an earlier course of the Trent and multiple channels, perhaps vestiges of an early Holocene braid-plain.

3.4 The Lower Trent Valley

LiDAR for the Upper Trent Valley was limited to a 6km long stretch of the Valley from the confluence of the Rivers Trent and Idle at West Stockwith downstream to immediately south of East Ferry, Lincolnshire.

The valley here is broad with subdued relief. The Trent-Idle confluence is overlooked on the south side by the higher Triassic Mercia Mudstone ridge around Walkeringham and Misterton, and on the north side by the southern edge of the Isle of Axholme. The mapped drift geology (Figure 30; Doncaster Sheet 88) comprises silt and clay alluvium in the valley floor (shown by boreholes to be up to 19m thick; TVG 2002 Component 3, Challis 2004) with the marginally higher Holme Pierrpont Sand and Gravel to the east. The Valley sides have a veneer of early Holocene aeolian sand with extensive peat deposits in Misterton Carr, to the west. Although not mapped, these peat deposits probably once blanketed most of the floodplain within the study area beneath a relatively insubstantial depth of silt and clay alluvium and artificially created warp.

The LiDAR DSM of the study area (Figure 31) provides a significant increase in the understanding of the geomorphology and geoarchaeology of the study area. The principal features evident on the DSM are the marked levee of the contemporary channel of the Trent (Figure 32) and a substantial, and hitherto unrecognised, rodden, with associated lesser creek ridges, deviating from the contemporary channel to the north-east and marking an earlier course of the Trent (Figure 33).

The presence of these marked topographical features suggests that the peat that once blanketed much of the floodplain has experienced significant desiccation and shrinkage, probably due to modern agricultural drainage. The relatively greater shrinkage of dry peat, compared to drying sand, silt and clay, leads to the relief inversion responsible for rodden and creek ridge formation, a phenomenon common in the East Anglian Fens and the Witham Valley (see section 6).

At the eastern edge of the DSM a number of circular features are revealed by the shrinking peat (Figures 33 and 34). These features lay at the extreme western edge of the Holme Pierrpont Sand and Gravel terrace, and may be no more than projecting irregularities in the terrace surface. However, their size, shape and disposition is reminiscent of Bronze Age round barrows, located at the fringes of the floodplain of the Trent and revealed by similar processes to those better documented examples in the Witham Valley in Lincolnshire (for example at Fiskerton, see section 6 and Figures 42 and 43). These features merit further investigation.

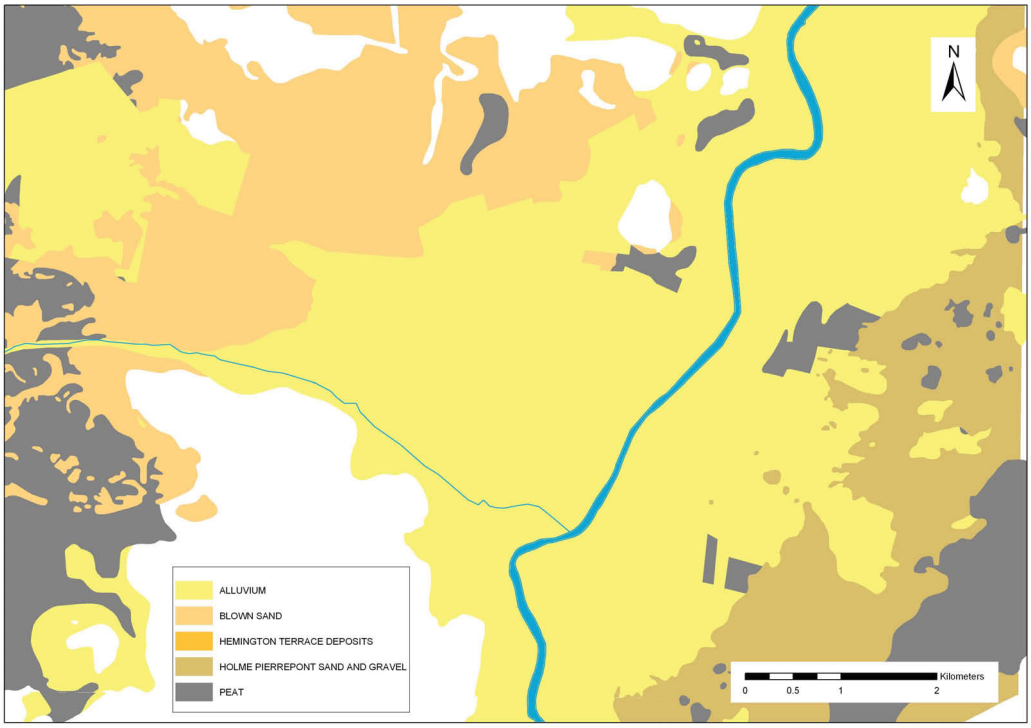

Figure 30. Map showing the drift geology of the Lower Trent Valley at the confluence of the Rivers Trent and Idle.

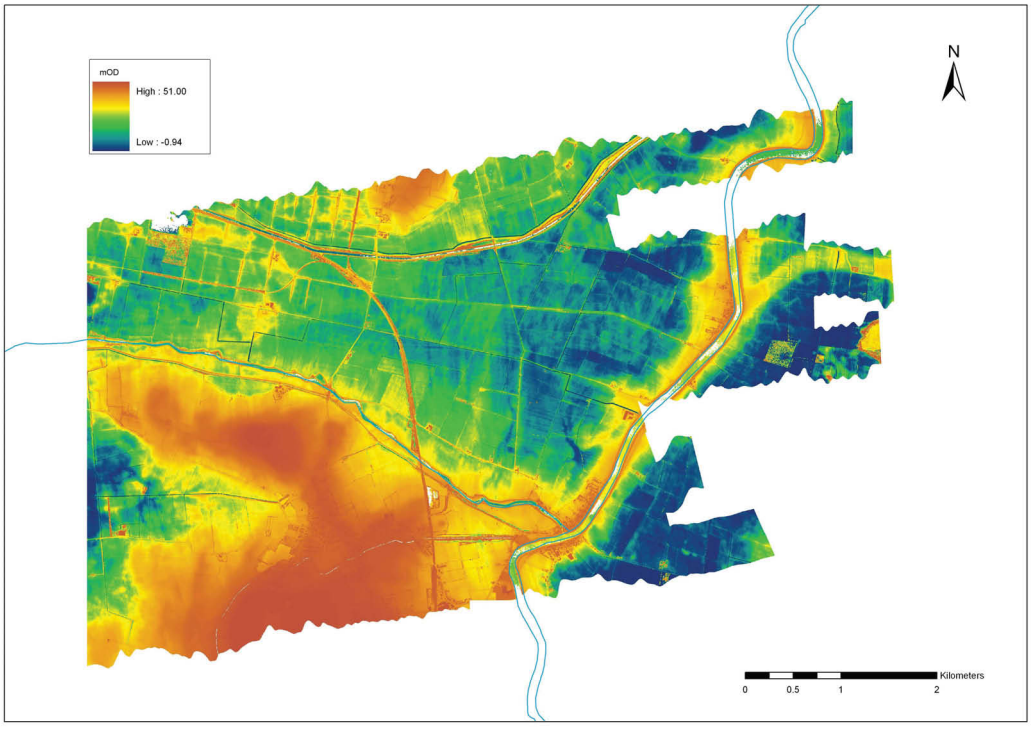

Figure 31. Colour-shaded LiDAR DSM of the Lower Trent Valley at the confluence of the Rivers Trent and Idle.

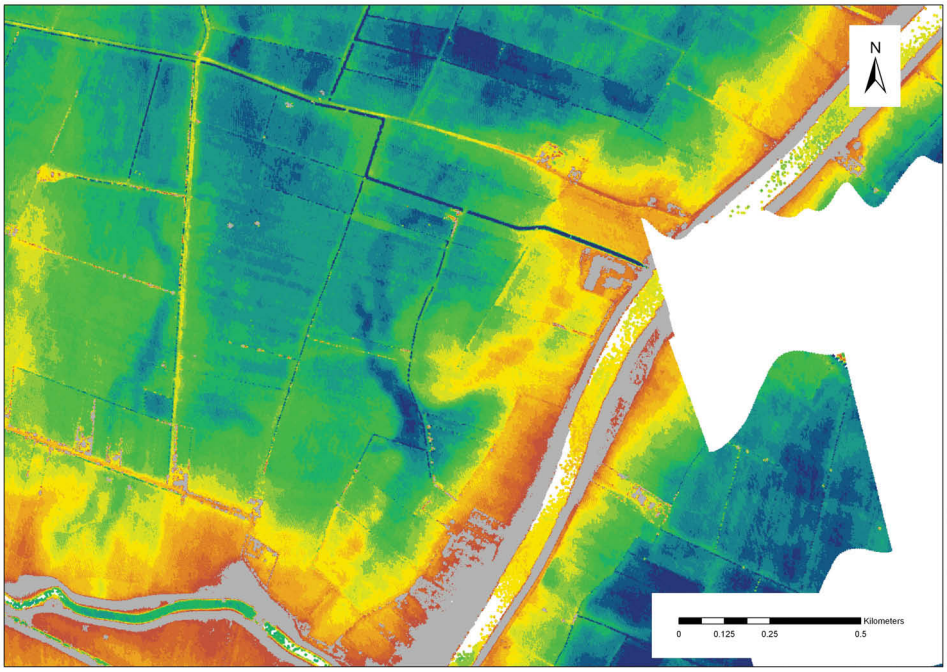

Figure 32. Colour-shaded LiDAR DSM of the Lower Trent Valley at the confluence of the Rivers Trent and Idle. The raised levee of the contemporary Trent channel and palaeodrainage features in the surrounding peatlands is clearly evident.

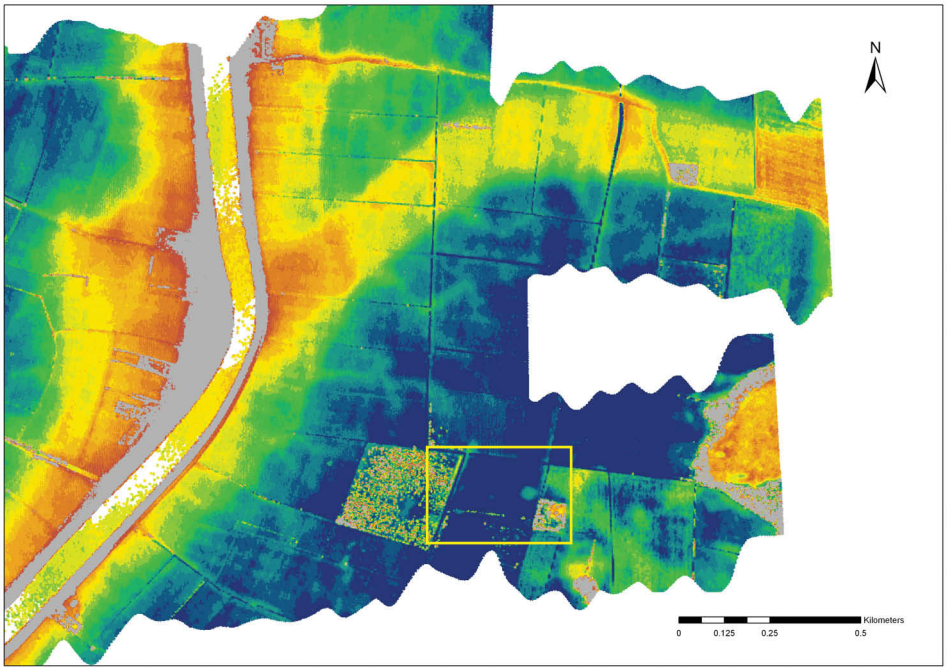

Figure 33. Colour-shaded LiDAR DSM of the Lower Trent Valley at the confluence of the Rivers Trent and Idle. A substantial rodden marking an earlier course of the River Trent is clearly visible. A number of circular features in the south-east of the image (within yellow square) are reminiscent of round barrows revealed by shrinking peat.

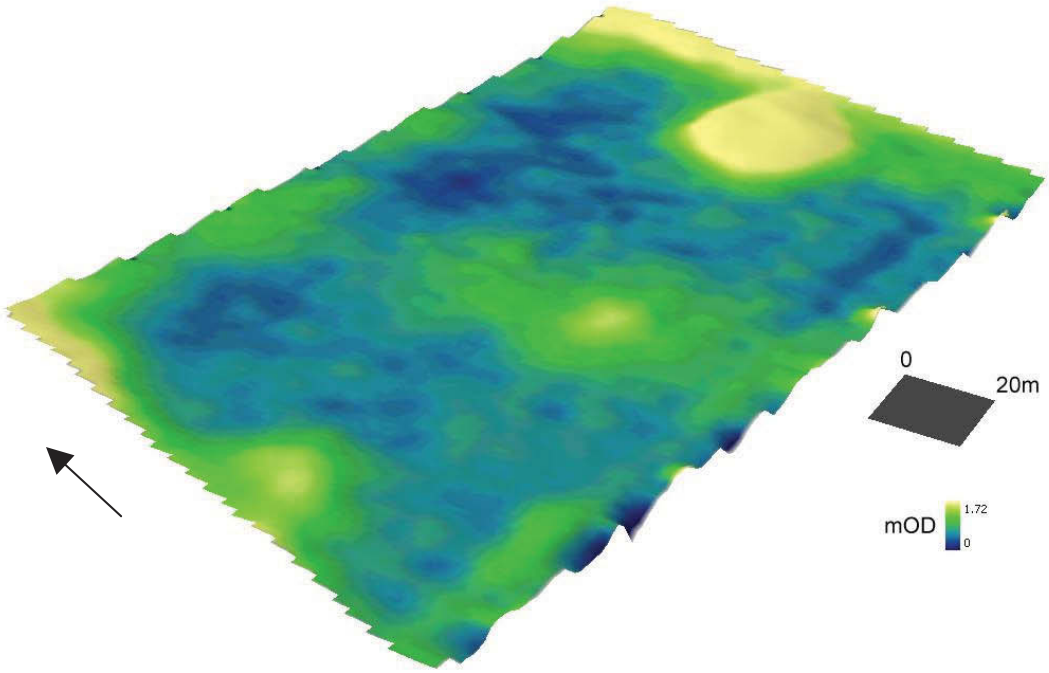

x5 vertical exaggeration

Figure 34. Colour-shaded pseudo-3D view of an extract from the LiDAR DSM of the Lower Trent Valley showing circular features reminiscent of round barrows revealed by shrinking peat (see Figure 33 for location of extract).

3.5 LiDAR in the Trent Valley: Some Conclusions

In the Trent Valley LiDAR has proven its worth as a tool for geoarchaeological prospection and mapping.

The middle reaches of the Trent, where the wide floodplain is dominated by lateral channel movement and a complex sequence of terraces survive, LiDAR is useful for mapping floodplain features of archaeological interest such as palaeochannels and reveals relict structural features of the gravel terraces.

Aspects of the historic landscape such as earthwork ridge and furrow are clearly evident, and careful examination of the LiDAR DSM reveals upstanding features that may indicate hitherto unrecognised monuments.

4 THE VALE OF YORK

4.1 Introduction

LiDAR data for the Vale of York was supplied by EA for the corridors of the Rivers Ouse, Wharfe, Foss, Nidd and Derwent as part of the English Heritage ALSF funded Vale of York Project (EH PNUM 3041). The geology of the Vale contrasts markedly with that of the Trent Valley making comparison of the LiDAR DSM for these two areas a useful and instructive exercise. In this report, two contrasting areas of the Vale of York, the River Ouse and The River Foss, are considered (Figure 35).

4.2 The Geology of the Vale of York *(by Andy J Howard)*

The Vale is a low-lying alluvial basin extending over 50 km from the vicinity of Northallerton in the north to the Doncaster-Gainsborough area in the south. During the last glacial maximum glacier ice entered the Vale of York and was joined by ice flowing down Swaledale, Wensleydale, Nidderdale and Wharfedale from local accumulation centres in what are now the Yorkshire Dales. Glacial and meltwater processes within and beneath the icesheet led to the deposition of extensive deposits of till and fluvioglacial sands and gravels. Ice flowing down the east coast blocked the Humber Estuary, resulting in drainage impediment and the creation of a large lake - Lake Humber – in front (i.e. to the south) of the glacier. The sediments formed in Lake Humber largely comprise laminated clays, with sands being deposited at the lake margins. These deposits, together with upper sands of post-lacustrine fluvial origin, are for historical reasons known collectively as the '25-Foot Drift'. The position of the ice margin during the later, prolonged low-level phase of Lake Humber is marked by surviving ridges of till, sand and gravel, known as moraines, which extend across the Vale of York from east to west in the vicinities of York and Escrick. The lake eventually disappeared as a result of silt accumulation rather than through drainage, and the upper sands of the 25-Foot Drift, which form low discontinuous ridges and mounds, are interpreted as levées deposited by rivers flowing across this newly-created land surface.

Between 11,000 and 10,000 years BP colder climatic conditions returned to the Vale of York, creating a tundra environment. Within this sparsely vegetated landscape, the finer grained fluvioglacial deposits and the upper sands of the 25-Foot Drift were subject to processes of wind erosion, creating extensive sheets of wind-blown ('aeolian') sand and dune landforms in the areas to the east and north of where the city of York now stands.

At the beginning of the post-glacial period, c.13,000 years BP, large volumes of water were still locked up within ice sheets, with the result that the contemporary sea level was much lower than it is today. Rivers flowing across areas of the Vale previously covered by glaciers therefore cut deep channels through the sediments of the former Lake Humber, to a depth of around –20 m OD. Through time, sea level rise resulted in the deposition of sediments which gradually infilled these incised river channels. Upstream of tidal influence, the low-gradient river systems of the Vale have been characterised during the Holocene by low rates of lateral movement and relatively high rates of fine-grained (sand, silt, clay and peat) sedimentation.

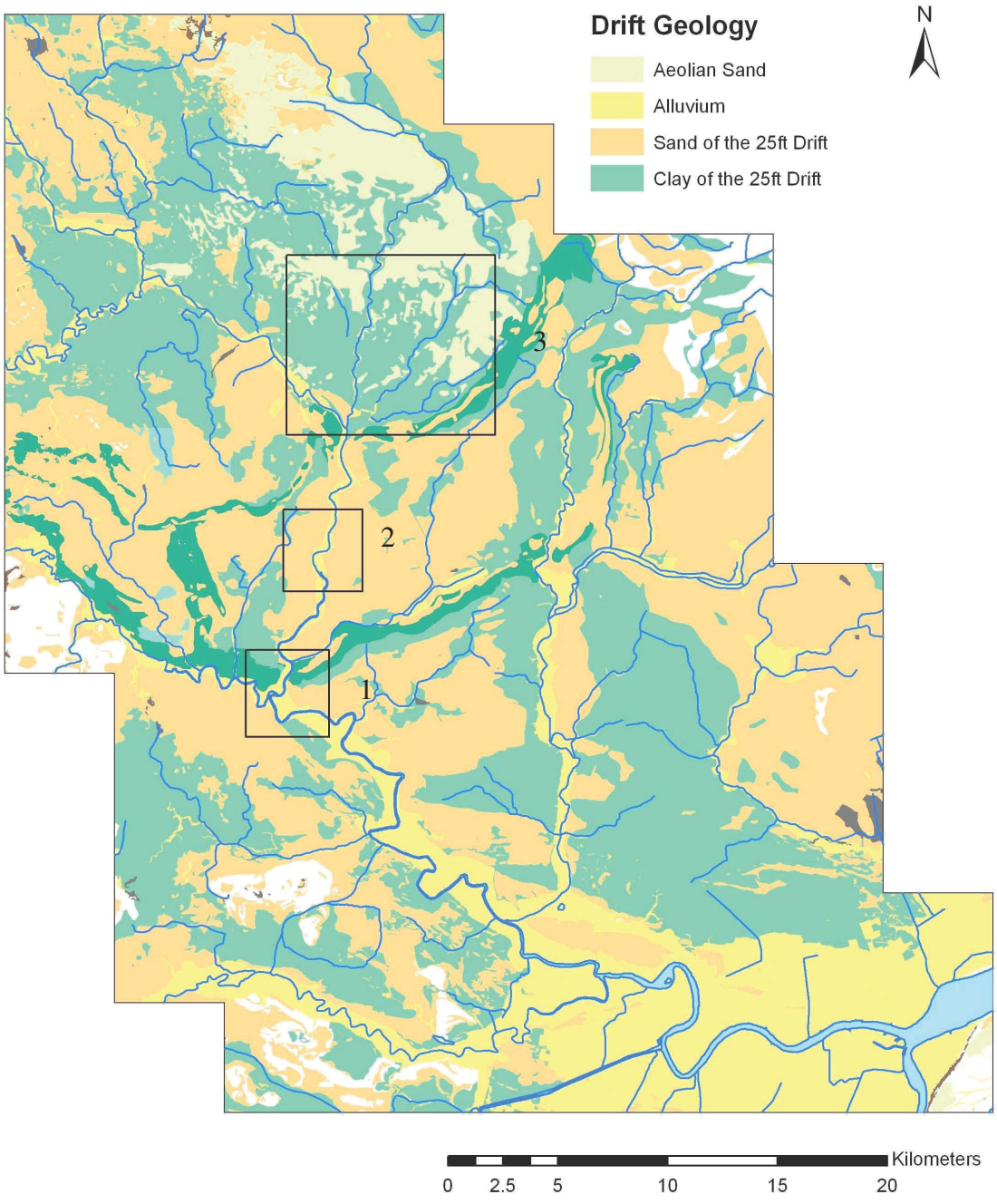

Figure 35. The drift geology of the Vale of York, showing the three LiDAR study areas discussed in the text: (1) the Ouse/Wharfe confluence (2) the Ouse at Naburn and (3) The River Foss.

4.3 The River Ouse

The Ouse is the principal river draining the Vale of York, rising on the north-western fringes of the Vale of York and flowing 80km south to its confluence with the Humber Estuary at Blacktoft. For most of its course the Ouse is constrained within a relatively narrow valley, although south of its confluence with the River Wharfe at Cawood the valley widens, broadening considerably beyond the confluence with the Derwent, where its assumes a perimarine character.

LiDAR DSM for two representative reaches of the Ouse at Cawood and Naburn are shown in Figures 36 and 37.

In both instances the narrow floodplain (barely 500m wide at Naburn) is dominated by fine-grained sedimentation, with little or no evidence for lateral channel movement preserved as palaeochannels. At Cawood (Figure 36) the most clearly defined features are the valleys of minor tributary streams of the Ouse and Wharfe (most now constrained and canalised to serve as field drains) the Escrick Moraine, and the valley of Stillingfleet Beck flanking the northern edge of the moraine. Some lower lying areas at the fringes of the Ouse floodplain, which are not mapped as floodplain or alluvium, appear to be sufficiently low-lying to have experienced periodic flooding.

At Naburn (Figure 37) the narrow valley of the Ouse is clearly described by the LiDAR DSM. Deposits flanking the valley are mapped as homogenous sand of the 25ft drift but show considerable topographical variation. When cropmarks (mapped by English Heritage as part of the National Mapping Programme for the Vale of York) are superimposed on the LiDAR DSM these variations in topography are seen to provide clear boundaries to the visibility of cropmarks. It seems likely that lower lying areas of 25ft drift sand include water retentive silt and clay deposits, perhaps deposited by overbank flooding either by the Ouse, or is minor tributaries, the valleys of which are once again quite clearly evident of the LiDAR DSM. These wetter areas may have retarded the formation of cropmarks, largely attributable to a later prehistoric and Romano-British settlement and field system, many of which appear to extend into blank areas in a manner suggesting the continued presence of their parent features. Some of the lower lying areas may indicate former river margin wetlands, themselves of potential archaeological interest.

4.4 The River Foss

The River Foss rises on the north-eastern fringes of the Vale of York near to Crayke, flowing 23km south and west to its confluence with the Ouse in York. For much of its course constrained in a very narrow valley, the Foss is of particular interest close to York, where the river channel has been heavily managed and the floodplain modified from the Roman period onward. Figure 38 shows the confluence of the Rivers Fosse and Ouse at York and the valleys of the Tang Hall and Osbaldwick Becks, minor tributaries of the Foss. The LiDAR DSM reveals much of the original topography of the Foss Valley, now largely submerged beneath suburban York. Of particular note is the low-lying basin close to the Ouse confluence; a vestige of the medieval King's Fishpond, an artificial lake created by damming of the Foss at this point. North and east of York the LiDAR DSM highlights the subtle topography of aeolian sand dunes. These dunes, the general disposition of which is mapped by the geological survey, are an important landscape feature in this area, affecting both archaeological visibility

(cropmark formation is largely confined to the better drained soils of the dunes) and also in some places burying or encapsulating cultural archaeological materials in reworked sand. The facility to rapidly and accurately map the locations and extent of these deposits provided by LiDAR is a significant contribution to understanding the archaeological landscape of this area.

4.5 LiDAR in the Vale of York: Some Conclusions

In the examples discussed here LiDAR in the Vale of York has been used principally to provide a detailed landscape context for archaeological study.

High resolution LiDAR DSM provide a detailed picture of topography that assisting in understanding complex aspects of the archaeological landscape such as the factors affecting cropmark formation, and variations in landscape character that may have affected settlement and activity choices and locations in the past.

LiDAR has been shown to contribute to a far higher level of understanding of the natural landscape than may be achieved by other sources of information, such as geology mapping or for that matter air-photography.

LiDAR data can assist in rapidly characterising large landscape areas, particularly when used in conjunction with other information sources, and assists in identifying prime target areas for field investigation.

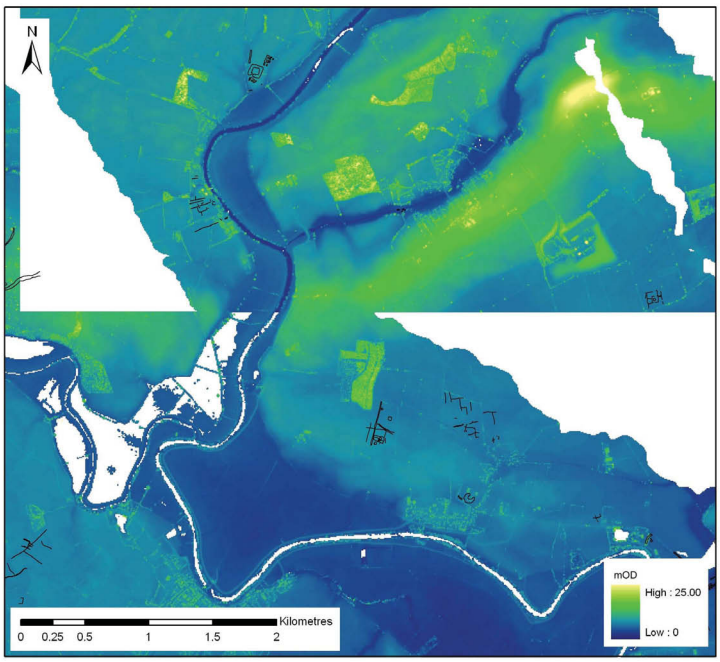

Figure 36. Colour-shaded LiDAR DSM of the confluence of the Rivers Wharfe and Ouse at Cawood. The floodplains of these two rivers are dominated by the accretion of fine-grained alluvial silt and clay and few palaeochannels are evident along their length. The linear ride of the Escrick moraine is clearly visible in the centre of the image.

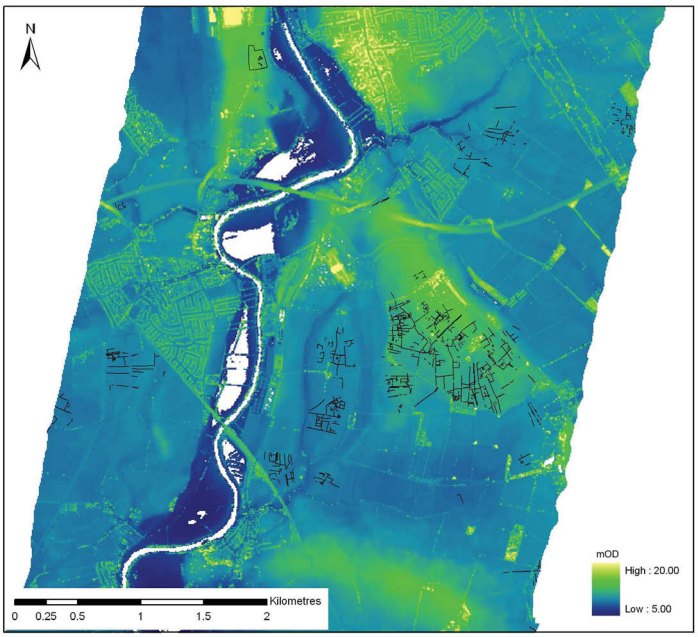

Figure 37. Colour-shaded LiDAR DSM of the Ouse Valley at Naburn., south of York with cropmarks from the English Heritage National Mapping Programme superimposed LiDAR clearly reveals subtle variations in the topography of the floodplain and terraces mirroring underlying geology and affecting cropmark formation.

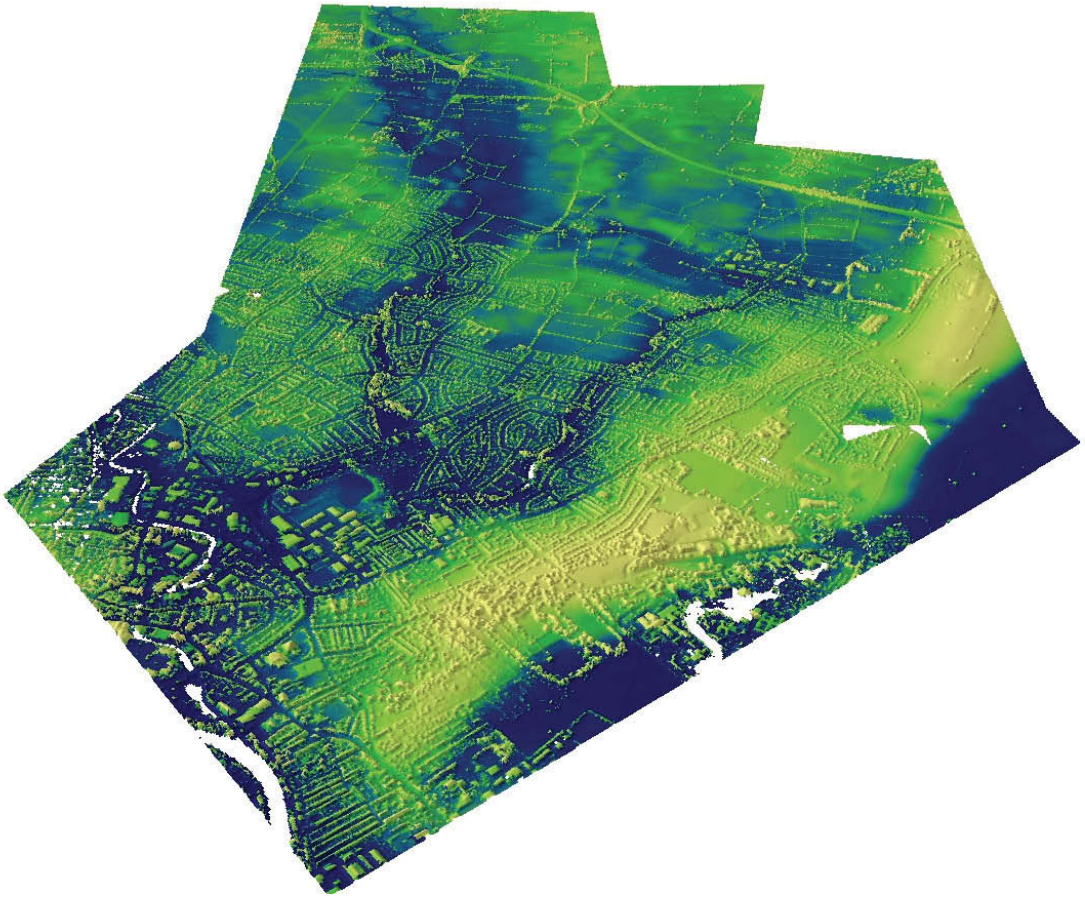

Figure 38. Colour-shaded pseudo-3d view of LiDAR DSM of the Valley of the River Foss and its tributaries the Osbaldwick Beck and Tang Hall Beck to the north-east of York. Details of these Valleys, largely submerged by the suburban growth of York, together with the subtle surface topography of aeolian dune deposits are evident.

5 THE WITHAM VALLEY

5.1 Introduction

LiDAR data for the Witham Valley was acquired from EA by Lincolnshire County Council as part of the English Heritage funded study of the archaeology of the Witham Valley (Catney and Start 2003). Some image processing was undertaken by the present author and this presented the opportunity to compare LiDAR data for the Witham Valley with other areas studied.

5.2 The Geology of the Witham valley

The River Witham rises at South Witham flowing for approximately 140km to The Wash, initially broadly north and east before turning south beyond the Lincoln Gap, and from Lincoln following a now largely canalised route to meet the Haven at Boston. The 35km length of the Witham Valley between Lincoln and Tattershall preserves a rare landscape of interface between fenland and river valley (French and Rackham 2003) with a complex and imperfectly understood post-glacial geology.

South of Lincoln, from Fiskerton, the largely canalised river follows the north side of the valley floor, a course occupied since the 11th century AD. A substantial depth of post-glacial sediment infills the valley including extensive marine sediments at the eastern end of the valley. Organic clays, silts and peat infilling the valley cover earlier land surfaces inundated by marine incursions and rise in river level. Elements of a dendritic estuarine creek system have been plotted from air-photographs and soil mapping. In later prehistory the sea retreated from the valley followed by the development of extensive peat deposits across the valley floor. From the 19th century drainage associated with extensive agriculture has led to the desiccation and gradual shrinkage of these peat deposits, once up to eight feet (2.4m) thick. As it has shrunk the peat has exposed the creek and channel systems of the prehistoric drainage network together with features of the contemporary archaeological landscape such as barrow fields, causeways and other structures.

5.3 Palaeodrainage of the Witham Valley

Figure 40 illustrates the extensive palaeodrainage system of roddens and creek ridges within the Witham Valley evidenced as slightly raised sinuous ridges of sand, silt and clay revealed by oxidation, deflation and shrinkage of desiccating peat. A complex dendritic pattern of, creeks and inlets, flanking a main channel probably beyond the south-western limit of LiDAR survey, but perhaps glimpsed in the extreme south-western corner of the image for Branston, suggests a landscape much like the undrained portions of The Wash.

5.4 Archaeology in the Witham Valley

Peat shrinkage has also served to reveal hitherto masked features of the prehistoric cultural landscape. At Barlings (Figure 41) a group of Bronze Age round barrows are revealed located on marginally higher land within a small tributary valley of the Witham, the LiDAR DSM may be usefully compared with published aerial

photography (Went 2003, fig 2) and serves to usefully illustrate not just the extent of the cemetery but also its detailed logographical setting. At Fiskerton (Figure 42) a further group of Bronze Age round barrows are revealed besides the Witham. The LiDAR DSM clearly delineates the complex geomorphology of the pre-canalisation channels of the River Witham and a minor tributary in a landscape that, though intermittently susceptible to air-photography (*cf* Catney and Start 2002, backcover) is revealed in great clarity by changes in elevation in the order of centimetres. The subdued topography of the river valley and the emerging barrow field is effectively illustrated through a pseudo-three-dimensional view of the barrows at Fiskerton (Figure 43), which serves to further emphasise the power of LiDAR data for archaeological prospection.

Finally, the uses of LiDAR DSM for three-dimensional mapping of even well-known earthwork monuments is revealed by the DSM of the deserted settlement at Woodhall Spar (Figure 44) which may be compared to vertical aerial photography of the same site. Here LiDAR provides a rapid mean to produce durable earthwork mapping) for example through automatically generated contours of the earthworks, or manually interpreted hachure. In addition subsequent LiDAR flights might provide a rapid and effective means of monitoring preservation and survival at this monument and the majority of other archaeological sites preserved as earthworks.

5.5 LiDAR in the Witham Valley: Some Conclusions

In the examples discussed LiDAR in the Witham Valley has been used principally to map the complex prehistoric palaeodrainage network.

LiDAR has also been used to identify Bronze Age round barrows revealed by shrinking peat and is particularly useful in placing individual monuments and groups of monuments in their broader landscape setting.

LiDAR data for a deserted medieval settlement illustrated the potential of the technique for rapid mapping of such monuments and the possibility of uses for monitoring preservation and erosion.

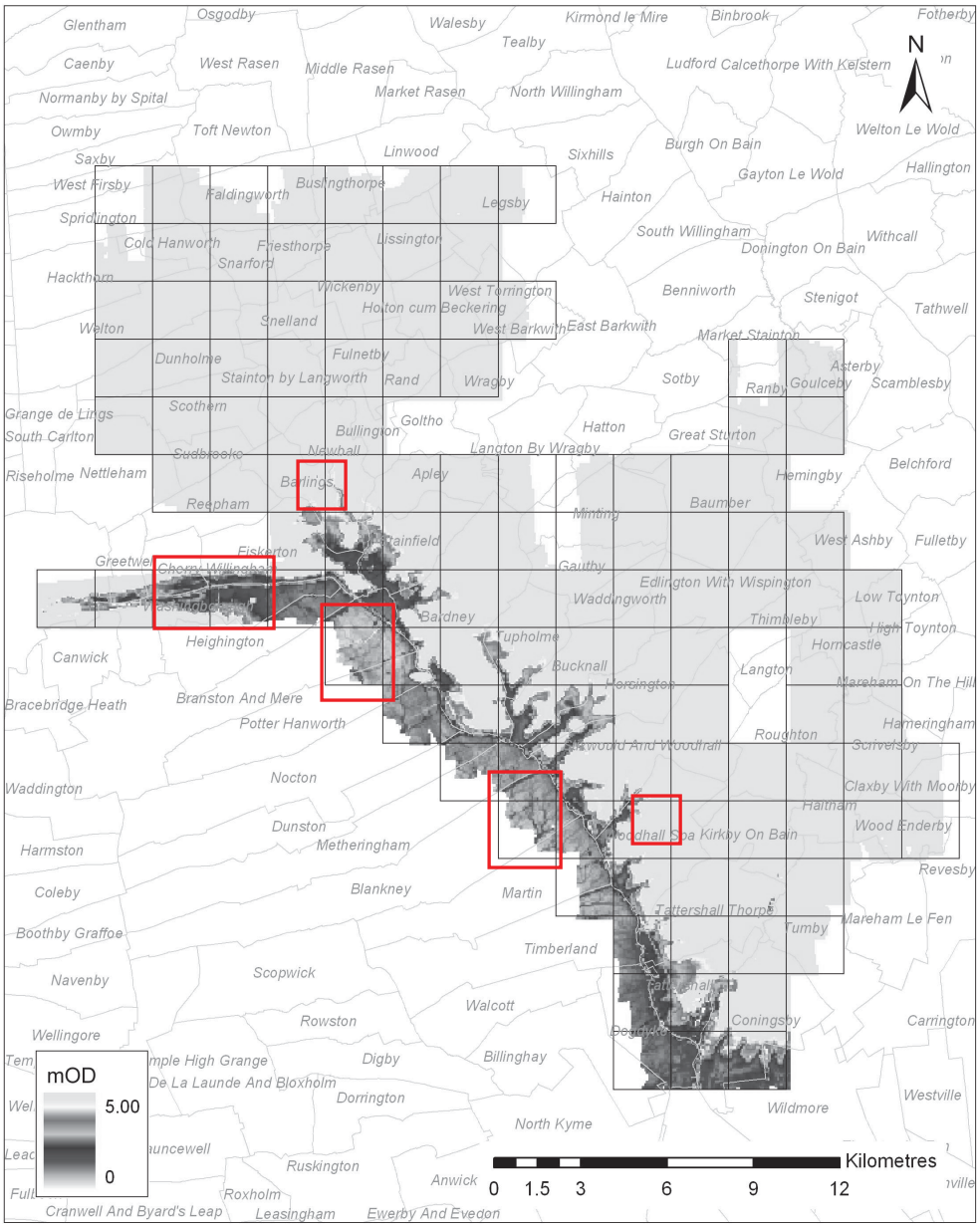

Figure 39. LiDAR coverage of the Witham Valley between Fiskerton and Conningsby shaded to show palaeodrainage in the valley floor. The detailed areas shown in Figures 40 to 44 are highlighted in red.

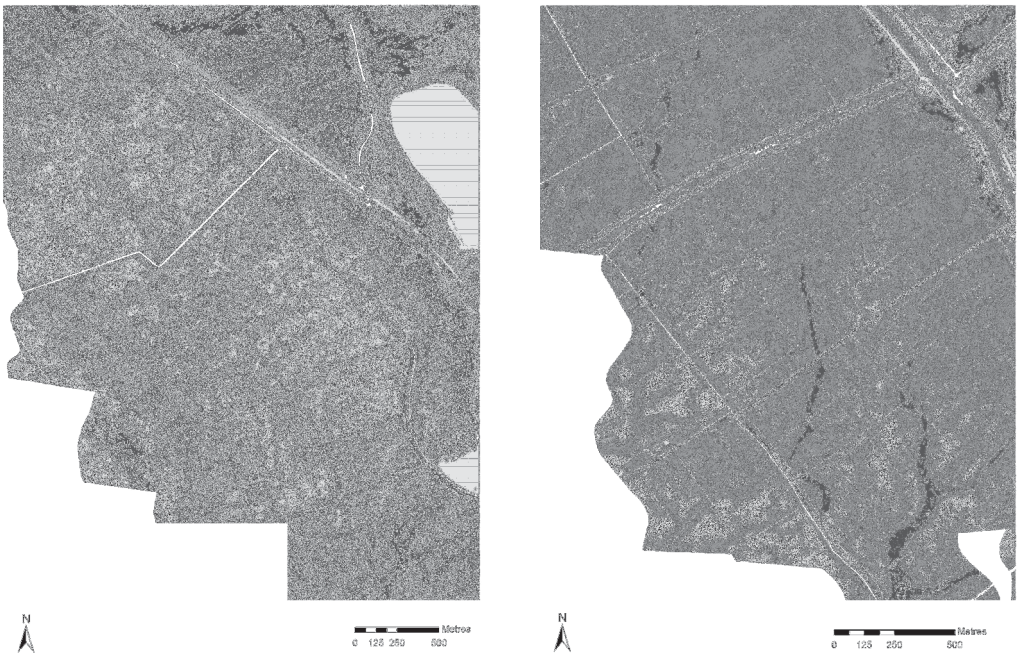

Figure 40. Greyscale LiDAR DSM of the Witham Valley at (left) Branston and (right) Blankney. A complex palaeodrainage system is revealed by slightly raised roddens and creek ridges emerging from the desiccating and shrinking peat that covers the floodplain.

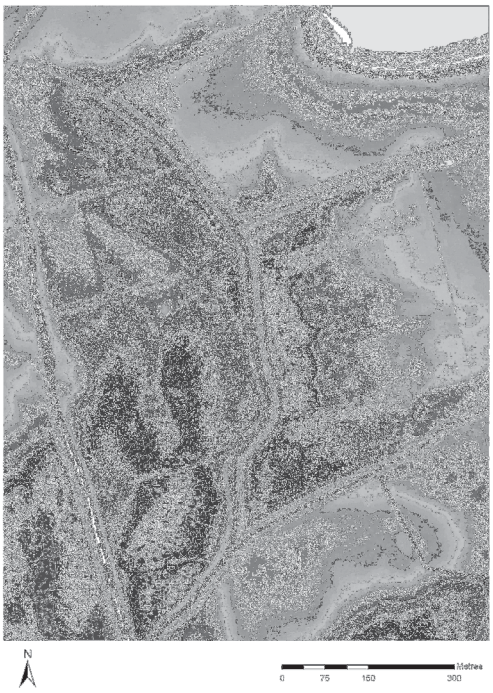

Figure 41. Greyscale LiDAR DSM of the Witham Valley. Bronze Age round barrows of the Barlings barrow cemetery are visible as raised (lighter colourer) areas.

Figure 42. Greyscale LiDAR DSM of the Witham Valley at Fiskerton. The complex geomorphology of the floodplain is clearly evident. A number of Bronze Age round barrows emerging from the desiccating and shrinking peat are visible as slightly raised (lighter coloured) areas in the south-east of the image. See Figure 30 for pseudo-3D view of outlined area.

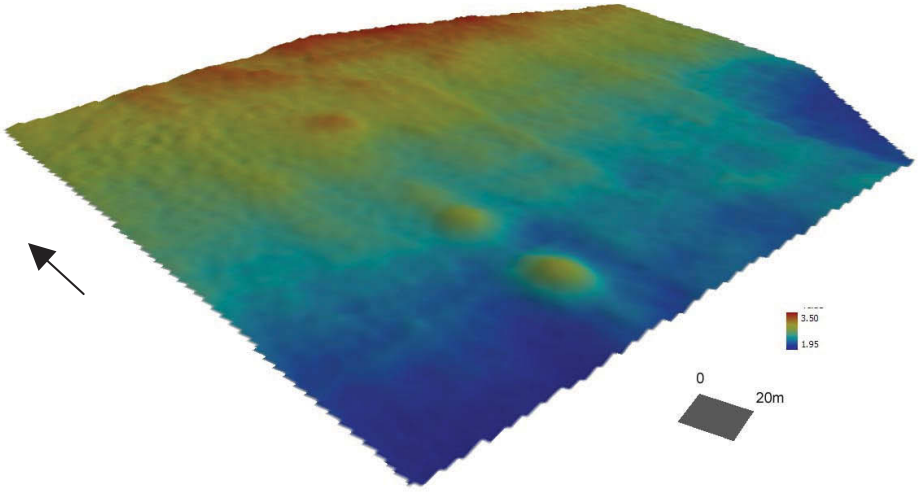

x 5 vertical exaggeration.

Figure 43. Colour-shaded pseudo-3D view of and extract of the LiDAR DSM of the Witham Valley showing the barrow group seen in Figure 42.

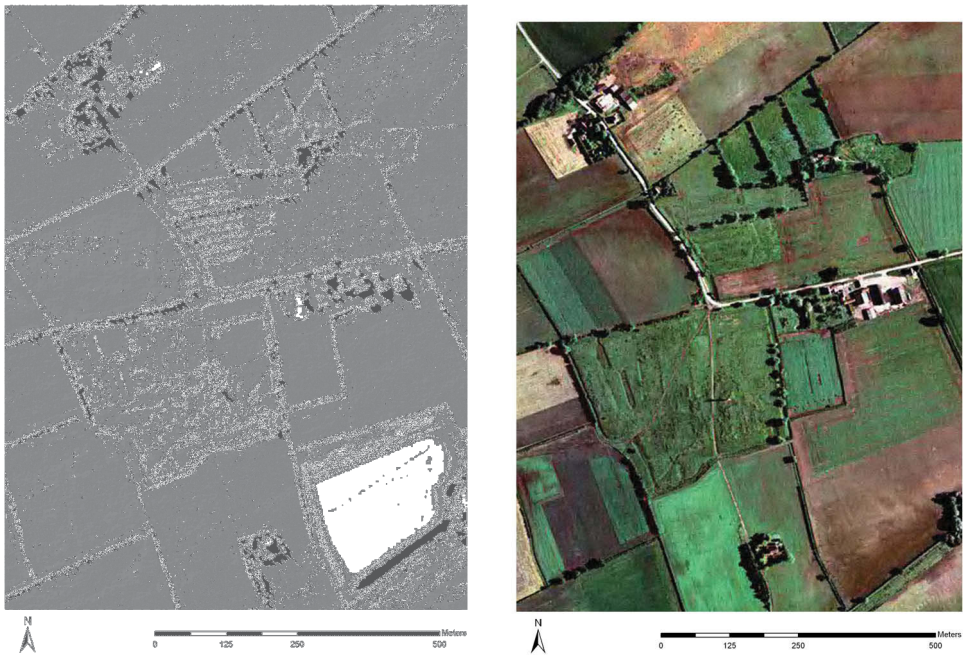

Figure 44. Woodhall Spar DMV, Lincolnshire. A comparison of solar-shaded LiDAR DSM and vertical air-photography shows the effectiveness of LiDAR for identifying and mapping archaeological earthworks.

6 CONCLUSIONS

This research report has sought to examine the uses and efficacy of LiDAR, principally that LiDAR data provided by EA, as a means for archaeological prospection in alluvial landscapes.

In general it is clear that LiDAR is particularly effective for mapping features of mature, middle reach floodplains dominated by lateral channel movement and desiccating peat dominated wetlands/floodplains. However, it is less effective in upper river reaches which are dominated by rapid erosion and little survival of paleolandscape features and in lower river reaches and where accretion is the dominant process

LiDAR is able to detect and allow mapping of archaeological earthworks and it offers considerable potential for assessing monument preservation through initial flights and revisits

LiDAR data provided by EA has some limitations. In particular the data is prone to artefacts introduced by interference at overlapping survey swath boundaries. This error should be removed during initial data processing by EA and its presence in the finished produce suggests deficiencies in data management and quality control that may be worth addressing. EA's filtered DTM data is not wholly reliable as a representation of the bare earth ground surface as it includes (often significant) interpolation artefacts. Some attempt was made to investigate alternative methods of producing bare earth DTM. High pass filtering of the DSM reduced swath overlap interference, but requires further investigation. Use of alternative methods of interpolation on data filtered using the EA provided mask may assist in overcoming some of the interpolation artefacts in the EA DTM. Simulating a first and last pulse DTM through selective filtering of the DSM is effective, so long as a reduced spatial resolution is acceptable in the final DTM. However, it is clear that for most application, including archaeological applications, access to raw point cloud, first and last pulse data is essential.

Automatic extraction of geoarchaeological features from the DSM proved all but impossible. The input of an experience analyst probably remains the fastest and most effective way for extracting information from LiDAR data.

The problems inherent in representing complex geomorphology features derived from continuous elevation data in a vector data model suggest that any digitised map layers produced from LiDAR are at best a summary to be used for alert mapping and should be supported by access to original LiDAR data, or at least raster images generated from LiDAR DSM, for detailed threat assessment.

Much remains to be done to fully assess the archaeological uses of LiDAR. Assessment of its effectiveness in other landscape (uplands, blanket peat bog and moorland, the intertidal zone, etc.) should be pursued. Rigorous examination of reflected pulse intensity data should be undertaken and the reliability of LiDAR as a tool for assessing preservation and erosion should be assessed by reflying previously surveyed areas (*cf* Barnes 2003). Finally, LiDAR might usefully be compared with

other off-the-shelf elevation products such as Interferometric Synthetic Aperture Radar (IFSAR; Hodgson *et al* 2002) which already offer 1m vertical resolution elevation data for the entire UK.

7 REFERENCES

Axelsson, P. 1999 'Processing of laser scanner data – algorithms and applications.' *ISPRS Journal of Photogrammetry & Remote Sensing* 54: 138-147

Barnes, I. 2003. 'Aerial remote-sensing techniques used in the management of archaeological monuments on the British army's Salisbury Plain training area, Wiltshire, UK' *Archaeological Prospection* 10: 83-90.

Baker, S. 2003. *The Trent Valley: Paleochannel Mapping from Aerial Photographs.* Trent Valley Geoarchaeology Research Report. Nottingham, Trent & Peak Archaeological Unit.

Bewley, Robert H. 2003 'Aerial survey for archaeology.' *The Photogrammetric Record* 18 (104), 273-292.

Brown, A.G., Keough, M.K. & Rice, R.J. 1994. 'Floodplain evolution in the East Midlands, United Kingdom: the Lateglacial and Flandrian alluvial record from the Soar and Nene valleys.' *Philosophical Transactions of the Royal Society, London.* A348: 261-293.

Brown, K., Duncan, A.' O'Dwyer, C., Davison, B., Hogarth, P,. Butler, D. & Sampson, E. 2003. 'Integrated airborne data collection by the Environment Agency.' In Aplin P. and Mather, P.M. (eds) *Proceedings of RSPSoc 2003: Scales and Dynamics in Observing the Environment, Nottingham, 10-12 September 2003*. Nottingham: The Remote Sensing and Photogrammetry Society.

Carney, J., Ambrose, K. and Brandon, A 2002 *Geology of the Loughborough district : a brief explanation of the geological map Sheet 141 Loughborough.* Keyworth, British Geological Survey.

Catney, S. and Start, D. (Eds) 2003. *Time and Tide. The Archaeology of the Witham Valley.* Sleaford. Witham Valley Archaeological Research Committee.

Challis, K. 2004. *Trent Valley GeoArchaeology 2002. Component 3 Alluvium Depth and Character Modelling.* Trent Valley Geoarchaeology Research Report. York, York Archaeological Trust.

Charlton, M.E., Large, A.R.G. and Fuller, I.C. 2003. 'Application of airborne LiDAR in river environments: the River Coquet, Northumberland, UK' *Earth Surface Processes and Landforms* 28: 299-306.

Cobby, D.M., Mason, D.C. and Davenport, I.J. 2001. 'Image processing of airborne scanning laser altimetry data for improved river flood modelling' *ISPRS Journal of Photogrammetry & Remote Sensing* 56: 121-138.

Dugdale, R.E. 1988. 'Geomorphology'. In Brazier, S. (ed) *A New Geography of Nottingham.* Trent Polytechnic, Nottingham.

Environment Agency. 1998. *Airborne light detection and range feasibility study.* National centre for Environmental data and Surveillance R&D Technical report E43. Environment Agency, Bristol.

French, C. and Rackham, J. 2003. 'Palaeoenvironmental research design for the Witham Valley.' In Catney, S. and Start, D. (Eds) 2003. *Time and Tide. The Archaeology of the Witham Valley.* Sleaford. Witham Valley Archaeological Research Committee: 33 – 42.

Garton, D. & Malone, S. 1998. 'Geomorphology from aerial photographs in the Trent Valley.' In Challis, K. (ed) Fieldwork by Trent & Peak Archaeological Trust in Nottinghamshire, 1996-7. *Transactions of the Thoroton Society of Nottinghamshire* 102. 139-141.

Goudie, A. 1990 *The Landforms of England and Wales.* Basil Blackwell, Oxford.

Gomes Pereira, L.M. and Wicherson, R.J. 1999 'Suitability of laser data for deriving geographical information a case study in the context of management of fluvial zones' *ISPRS Journal of Photogrammetry & Remote Sensing* 54: 105-114.

Guenther, G.C., Brooks, M.W. & LaRocque, P.E. 2000 'New capabilities of the "SHOALS" airborne Lidar bathymeter.' *Remote Sensing of Environment.* 73:247-255.

Haala, N. and Brenner, C. 1999 'Extraction of buildings and trees in urban environments.' *ISPRS Journal of Photogrammetry & Remote Sensing* 54: 130-137.

Havelock, G. and Howard, A.J. 2004 *Extending and Protecting Palaeoenvironmental Data: Deposit Sampling Interim Report.* Trent valley GeoArchaeology 2002 Research Report. Newcastle, Dept of Geography, University of Newcastle upon Tyne.

Hodgson, M.E., Jensen, J.R., Schmidt, L. Schill, S. & Davis, B. 2002 'An evaluation of LIDAR- and IFSAR-derived digital elevation models in leaf-on conditions with USGS Level 1 and Level 2 DTMs.' *Remote Sensing of Environment* 84: 295-308.

Howard, A.J. and Macklin, M.G. 1999. 'A generic geomorphological approach to archaeological interpretation and prospection in British river valleys: a guide for archaeologists investigating Holocene landscapes' *Antiquity* 73: 527-541,

Jaafar, J., Priestnall, G., Mather, P.M. & Viera, C.A. 1999. Construction of DTM from LiDAR DSM using Morphological Filtering, Conventional Statistical Approaches and Neural Networks. In P. Pan, & M. Barnsley (eds) *Earth Observation: From Data to Information*. Proceedings of the 25th Annual Conference and Exhibition of the Remote Sensing Society: 299-306.

Knight, D. & Howard, A.J. 1995 *Archaeology and alluvium in the Trent Valley: an archaeological assessment of the floodplain and gravel terraces.* Trent & Peak Archaeological Trust, Nottingham.

Lloyd, C.D and Atkinson, P.M. 2002. 'Deriving DSM from LiDAR data with kriging' *International Journal of Remote Sensing.* Vol 23 No12: 2519-2524.

Lohani, B. and Mason, D.C. 2001. 'Application of airborne scanning laser altimetry to the study of tidal channel geomorphology' *ISPRS Journal of Photogrammetry & Remote Sensing* 56: 100-120.

Marks, K. and Bates, P. 2000. 'Integration of high-resolution topographic data with floodplain flow models' *Hydrological Processes* 14: 2109-2122.

Mather, Paul. M. 1999. *Computer Processing of Remotely Sensed Images*. London: John Wiley and Sons.

McCullough, M.J. 1988. 'Terrain and surface modelling systems: theory and practice. 'P*hotogrammetric Record* 12 (72):747-99.

Mitas, L. & Mitasova, H. 1999 'Spatial Interpolation.' In Longley, P.A., Goodchild, M.F., Maguire, D.J. & Rhind, D.W. (eds) *Geographical Information Systems*. Vol1 Principles and Technical Issues. John Wiley & Sons, New York. 481-492.

Oliver, M.A. & Webster, R. 1990. 'Kriging: a method of interpolation for geographical information systems.' *International Journal of Geographical Information Systems,* 4 (3): 313-32.

Optech 2003 *ALTM 2033 Airborne Laser Terrain Mapper.* Optech, Toronto.

Priestnall, G., Jaafar, J. and Duncan, A. 2000. "Extracting urban features from LiDAR digital surface models" *Computers, Environment and Urban Systems* 24: 65-78.+

Rango, A., Chopping, M., Ritchie, J., Havstad, K., Kustas, W. & Schmugge, T. 2000 'Morphological characteristics of shrub coppice dunes in desert grasslands of southern New Mexico derived from scanning LIDAR.' *Remote Sensing of Environment* 74:26-44.

Straw, A. 2002. 'Lincolnshire gaps and more gaps.' *Geology Today* Vol 18 No 1: 17-22.

Went, D. 2003 'Management through other mechanisms.' In Catney, S. and Start, D. (Eds) 2003. *Time and Tide. The Archaeology of the Witham Valley.* Sleaford. Witham Valley Archaeological Research Committee: 52-59.

Wehr, A. and Lohr, U. 1999. 'Airborne laser scanning – an introduction and overview' *ISPRS Journal of Photogrammetry & Remote Sensing* 54: 68-82.

ACKNOWLEDGEMENTS

Access to LiDAR data for the Trent Valley and the Yale of York was kindly arranged by Andrew Heaton and Martin Fuller of the Environment Agency. Liz Sampson and Paul Hodkinson of the National Centre for Environmental Data and Surveillance coordinated the considerable task of extracting a large volume of LiDAR data from the Agency's archive.

At Lincolnshire County Council Mark Bennett and Steve Catney provided access to LiDAR data of the Witham Valley acquired for their research.

Data from Infoterra was processed at Birmingham University by Steven Wilkes, who also contributed much to discussing the technical details, processing methods and limitations of LiDAR.

Work was carried out as part of the Trent Valley GeoArchaeology 2002 and Alluvial Archaeology in the Vale of York projects funded by English Heritage through the Aggregates Levy Sustainability Fund (PN3307 and 3041). Thanks are expressed to the English Heritage project officer for these two projects, Jonathan Last, and to Mike Bishop the TVG group convener for their efforts in facilitating this undertaking.

YORK ARCHAEOLOGICAL TRUST

York Archaeological Trust undertakes a wide range of urban and rural archaeological consultancies, surveys, evaluations, assessments and excavations for commercial, academic and charitable clients. It can manage projects, provide professional advice and monitor archaeological works to ensure high quality, cost effective archaeology. Its staff have a considerable depth and variety of professional experience and an international reputation for research, development and maximising the public, educational and commercial benefits of archaeology. Based in York its services are available throughout Britain and beyond.

York Archaeological Trust
Cromwell House
13 Ogleforth
York YO1 7FG

Telephone: 01904 663000
Fax: 01904 663024
E-mail: enquiries@yorkarchaeology.co.uk
Internet: http://www.yorkarchaeology.co.uk

York Archaeological Trust is a
Registered Charity, No. 509060

A company limited by
guarantee without share capital
Registered in England No. 1430801